

## The mineralogy and fabric of 'Brickearths' in Kent, UK and their relationship to engineering behaviour

Milodowski, AE; Northmore, KJ; Kemp, SJ; Entwisle, DC; Gunn, DA; Jackson, PD; Boardman, David; Zoumpakis, Aris; Rogers, Christopher; Dixon, N; Jefferson, Ian; Smalley, IJ; Clarke, M

DOI:

[10.1007/s10064-014-0694-5](https://doi.org/10.1007/s10064-014-0694-5)

License:

Creative Commons: Attribution (CC BY)

### Document Version

Publisher's PDF, also known as Version of record

### Citation for published version (Harvard):

Milodowski, AE, Northmore, KJ, Kemp, SJ, Entwisle, DC, Gunn, DA, Jackson, PD, Boardman, D, Zoumpakis, A, Rogers, C, Dixon, N, Jefferson, I, Smalley, IJ & Clarke, M 2015, 'The mineralogy and fabric of 'Brickearths' in Kent, UK and their relationship to engineering behaviour', *Bulletin of Engineering Geology and the Environment*, vol. 74, no. 4, pp. 1187-1211. <https://doi.org/10.1007/s10064-014-0694-5>

[Link to publication on Research at Birmingham portal](#)

### Publisher Rights Statement:

The Author(s) 2015. This article is published with open access at Springerlink.com

### General rights

Unless a licence is specified above, all rights (including copyright and moral rights) in this document are retained by the authors and/or the copyright holders. The express permission of the copyright holder must be obtained for any use of this material other than for purposes permitted by law.

- Users may freely distribute the URL that is used to identify this publication.
- Users may download and/or print one copy of the publication from the University of Birmingham research portal for the purpose of private study or non-commercial research.
- User may use extracts from the document in line with the concept of 'fair dealing' under the Copyright, Designs and Patents Act 1988 (?)
- Users may not further distribute the material nor use it for the purposes of commercial gain.

Where a licence is displayed above, please note the terms and conditions of the licence govern your use of this document.

When citing, please reference the published version.

### Take down policy

While the University of Birmingham exercises care and attention in making items available there are rare occasions when an item has been uploaded in error or has been deemed to be commercially or otherwise sensitive.

If you believe that this is the case for this document, please contact [UBIRA@lists.bham.ac.uk](mailto:UBIRA@lists.bham.ac.uk) providing details and we will remove access to the work immediately and investigate.

# The mineralogy and fabric of ‘Brickearths’ in Kent, UK and their relationship to engineering behaviour

Antoni E. Milodowski · Kevin J. Northmore · Simon J. Kemp · David C. Entwisle · David A. Gunn · Peter D. Jackson · David I. Boardman · Aris Zoumpakis · Christopher D. F. Rogers · Neil Dixon · Ian Jefferson · Ian J. Smalley · Michèle Clarke

Received: 8 October 2014 / Accepted: 9 October 2014 / Published online: 14 March 2015  
© The Author(s) 2015. This article is published with open access at Springerlink.com

**Abstract** Mineralogical and petrographical investigation of two loessic brickearth profiles from Ospringe and Pegwell Bay in north Kent, UK have differentiated two types of brickearth fabric that can be correlated with different engineering behaviour. Both sequences comprise metastable (collapsing) calcareous brickearth, overlain by non-collapsing ‘non-calcareous’ brickearth. This study has demonstrated that the two types of brickearth are discretely different sedimentary units, with different primary sedimentary characteristics and an erosional junction between the two units. A palaeosol is developed on the calcareous brickearth, and is associated with the formation of rhizolithic calcrete indicating an arid or semi-arid environment. No evidence has been found for decalcification being responsible for the fabric of the upper ‘non-calcareous’ brickearth. Optically-stimulated dates lend further

support for the calcareous and ‘non-calcareous’ brickearth horizons being of different age or origins. The calcareous brickearth is metastable in that it undergoes rapid collapse settlement when wetted under applied stresses. It is characterised by an open-packed arrangement of clay-coated, silt-sized quartz particles and pelletised aggregate grains (peds) of compacted silt and clay, supported by an interped matrix of loosely packed, silt/fine-grained sand, in which the grains are held in place by a skeletal framework of illuviated clay. The illuviated clay forms bridges and pillars separating and binding the dispersed component silt/sand grains. There is little direct grain-to-grain contact and the resultant fabric has a very high voids ratio. Any applied load is largely supported by these delicate clay bridge and pillar microfabrics. Collapse of this brickearth fabric can be explained by a sequence of processes involving: (1) dispersion and disruption of the grain-bridging clay on saturation, leading to initial rapid collapse of the loose-packed interped silt/sand; (2) rearrangement and closer stacking of the compact aggregate silt/clay peds; (3) with increasing stress further consolidation may result from deformation and break up of the peds as they collapse into the interped regions. Smectite is a significant component of the clay assemblage and will swell on wetting, further encouraging disruption and breaking of the clay bonds. In contrast, the ‘non-calcareous’ brickearth already possesses a close-packed and interlocking arrangement of silt/sand grains with only limited scope for further consolidation under load. Minor authigenic calcite and dolomite may also form meniscus cements between silt grains. These have either acted as “scaffolds” on which illuviated clay has subsequently been deposited or have encrusted earlier-formed grain-bridging clay. In either case, the carbonate cements may help to reinforce the clay bridge fabrics. However, these carbonate features are a relatively minor

---

A. E. Milodowski (✉) · K. J. Northmore · S. J. Kemp · D. C. Entwisle · D. A. Gunn · P. D. Jackson  
British Geological Survey, Environmental Science Centre,  
Keyworth, Nottingham NG12 5GG, UK  
e-mail: aem@bgs.ac.uk

D. I. Boardman · A. Zoumpakis · C. D. F. Rogers · I. Jefferson  
School of Civil Engineering, The University of Birmingham,  
Edgbaston, Birmingham B15 2TT, UK

N. Dixon  
School of Civil and Building Engineering, Loughborough  
University, Loughborough, Leicestershire LE11 3TU, UK

I. J. Smalley  
Department of Geography, Leicester University,  
Leicester LE1 7RH, UK

M. Clarke  
School of Geography, University of Nottingham, University  
Park, Nottingham NG7 2RD, UK

feature and not an essential component of the collapsible brickearth fabric. Cryoturbation and micromorphological features indicate that the calcareous brickearth fabric has probably been developed through periglacial freeze–thaw processes. Freezing could have produced the compact silt/clay aggregates and an open porous soil framework containing significant inter-ped void space. Silt and clay were remobilised and translocated deeper into the soil profile by water percolating through the active layer of the sediment profile during thawing cycles, to form the loosed-packed inter-ped silt matrix and grain-bridging meniscus clay fabrics. In contrast, the upper ‘non-calcareous’ brickearth may represent a head or solifluction deposit. Mass movement during solifluction will have destroyed any delicate grain-bridging clay microfabrics that may have been present in this material.

**Keywords** Loess · Brickearth · Mineralogy · Fabric · Collapse behaviour · Palaeoenvironment

## Introduction

Loess and loessic soils are aeolian deposits typically consisting of highly porous soil fabrics dominated by silt-sized quartz particles. In the UK, Quaternary loessic deposits occur as discontinuous ‘spreads’ across southern and eastern England, and parts of Wales and the English Midlands (Fig. 1), and are variably represented on British Geological Survey maps as ‘*Brickearth*,’ ‘*Head Brickearth*,’ ‘*Head Silt*’ or as specific local formations such as the ‘*Enfield Silt*,’ ‘*Crayford Silt*’ and ‘*Langley Silt*.’ The nature and composition of these loessic brickearths bear close similarities to the much thicker and widespread loess deposits found in abundance in the major loess regions of North and South America, Europe including western Russia, Central Asia and China. In the UK, substantial thicknesses (>1 m) are generally restricted to north and east Kent (Pitcher et al. 1954; Fookes and Best 1969; Derbyshire and Mellors 1988), south Essex (Northmore et al. 1996) and the Sussex coastal plains (Catt 1977, 1988; Ballantyne and Harris 1993). Up to 8 m of brickearth have been found filling buried erosional channels in Essex, although thicknesses of 4 m or less are more common (Northmore et al. 1996). Most of the exposed loess/brickearth soils in Britain are probably of late Devensian age, deposited largely during the Dimlington Stadial (c. 14,000 to 25,000 years BP) and to a lesser extent during the Loch Lomond Stadial (10,000 to 11,000 BP) (Kerney 1965; Catt 1977; Ballantyne and Harris 1993; Antoine et al. 2003). A gradual southward and westward decrease in particle size, together with heavy mineral and other mineral tracer studies suggest the loess of eastern and southeastern England was deposited by

northeasterly winds. These re-worked silt materials are from outwash sandurs and glacial deposits around the North Sea Basin lobe of the Late Devensian ice-sheet (cf. discussions in Ballantyne and Harris 1993 and Antoine et al. 2003 and references therein). Subsequent re-working of these aeolian sediments through solifluction, colluvial and alluvial processes has produced a range of deposits variously described as ‘*brickearth*,’ ‘*head brickearth*,’ ‘*river brickearth*’ or ‘*loam*’ (Dines et al. 1954; Ballantyne and Harris 1993; Bell et al. 2003; Jefferson et al. 2003). Some loess was also deposited during the Early Devensian and pre-Ipswichian periods (Parks and Rendell 1992). The deposits may once have been extensive, but as a result of erosion and re-working they are now preserved only as isolated remnants; for example, in Jersey or in dolines in the chalk of the Chiltern Hills (Parks and Rendell 1988, 1992; Antoine et al. 2003; Bates et al. 2003).

Loess and loessic soils characteristically possess highly porous metastable grain fabrics with relatively low densities, and commonly have void space in their undisturbed state sufficient to hold their liquid limit water content at saturation (Bell and Culshaw 2001; Jefferson et al. 2001; Bell et al. 2003). Normally these materials are well drained and, while in their natural, low-water content phase, possess high apparent strength. However, they have the potential to undergo rapid collapse and settlement when saturated under applied loads, a process referred to as hydroconsolidation or hydrocollapse (Derbyshire et al. 1994; Klukanova and Sajgalik 1994; Rogers et al. 1994).

Although a less significant problem in the UK than in other loess regions of the world, loess collapse still causes damage locally with significant financial repercussions (Cattell 1997). However, not all loess brickearth deposits display collapse behaviour, and the mechanisms of loess metastability and subsequent collapse potential are still not fully understood (Derbyshire and Mellors 1988; Gao 1988; Bell et al. 2003 and references therein). It is important, therefore, that ground investigations in loessic brickearth deposits are focussed on establishing the distribution and thickness of these materials and, in particular, on identifying and characterising zones that are potentially metastable across a site within which engineering works are planned.

To further understand the collapse behaviour, and to develop techniques for defining the distribution of collapsible loessic deposits, a NERC-funded research study (involving a monitored field collapse test) was undertaken within loessic brickearth deposits at Ospringe in north Kent (Northmore et al. 2008; Gunn et al. 2006; Jackson et al. 2006; Zourmpakis et al. 2006). As part of this research programme, the mineralogical and petrographical characteristics of the brickearth from this site were investigated, together with supporting observations from other brickearth localities in southeast England (Fig. 1), to help

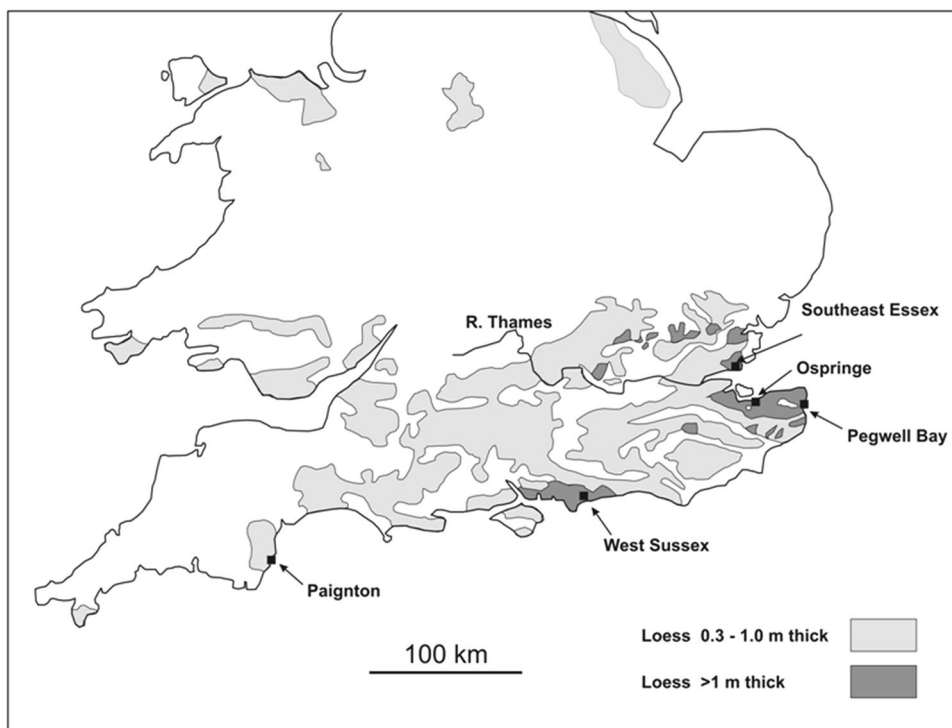


**Fig. 1** Distribution of Quaternary loess deposits in southern Britain (based on data from Catt 1977, 1988) and locations of 'Brickearth' sampling and study sites

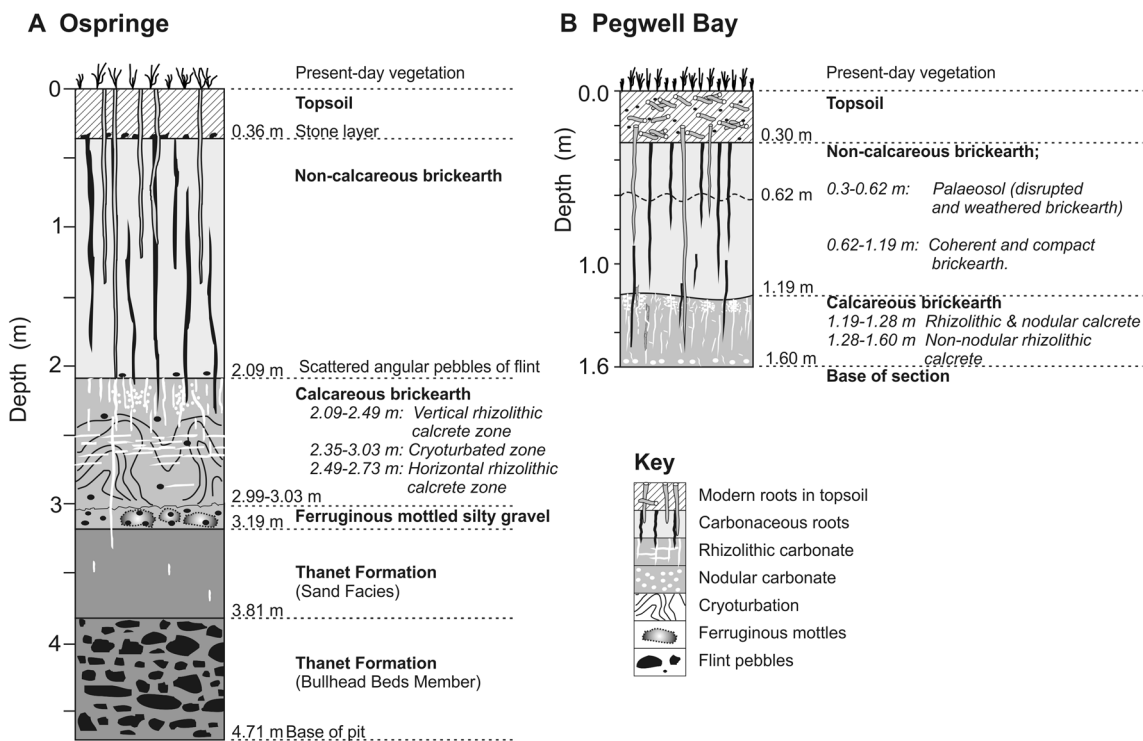


**Fig. 2** Summary lithological profiles for the Brickearth sequences at (a) Ospringe Pit 1 and (b) Cliffend, Pegwell Bay

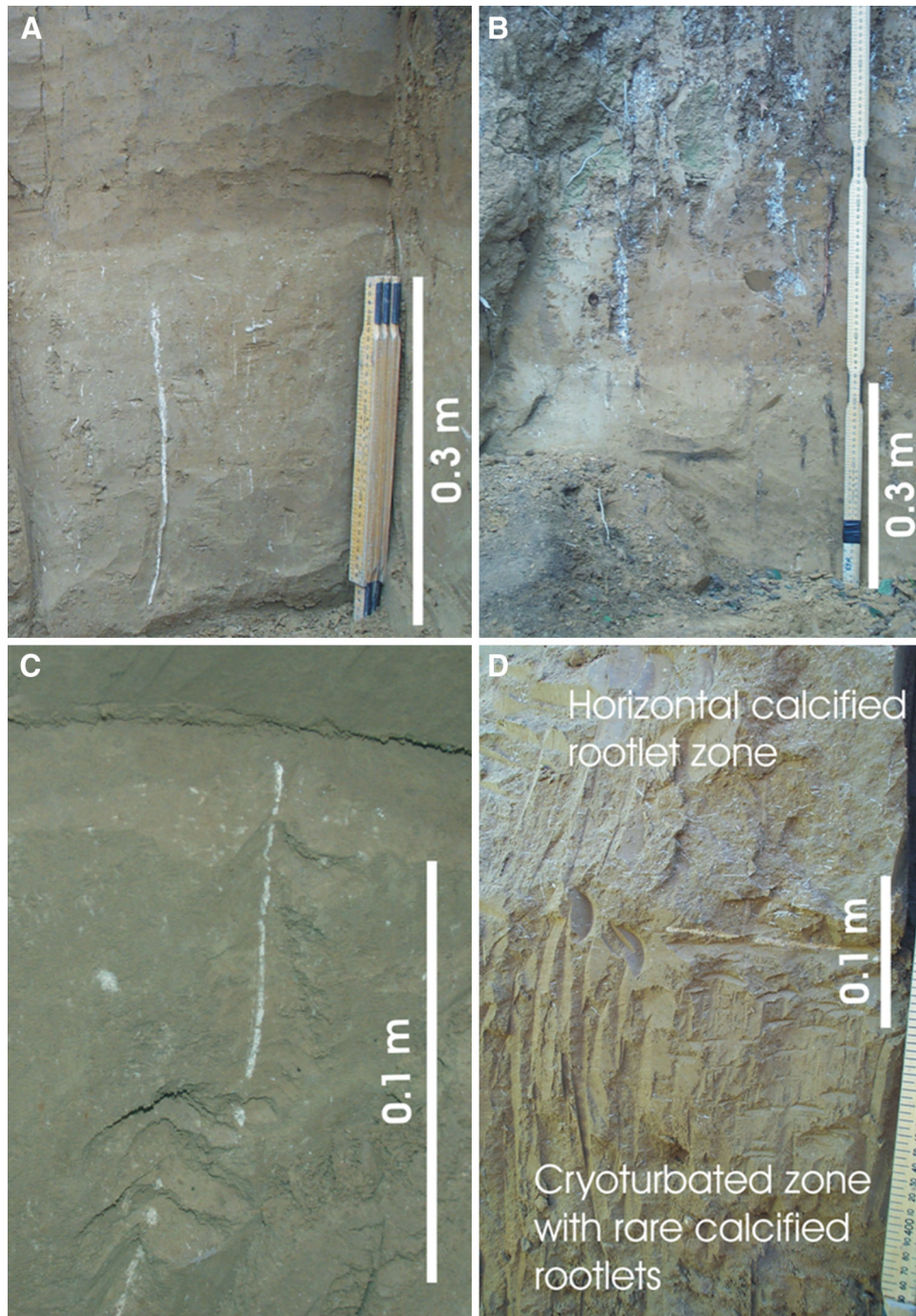


**Fig. 3** Photographs showing **a–b** a very sharp undulating erosional interface and marked colour difference between the light olive-brown upper ‘non-calcareous’ brickearth and the lower pale yellowish brown to yellowish-grey calcareous brickearth. **a** Ospringe, Pit 1. **b** Cliffend, Pegwell Bay. **b** The upper ‘non-calcareous’ brickearth is penetrated by open, old vertical root channels partially occupied by residual carbonaceous organic matter, that are lined and surrounded by

powdery white needle-fibre calcite. **c** White subvertical densely-calcified root structures can be seen in the lower calcareous brickearth which are truncated at the erosional interface, defining the base of the ‘non-calcareous’ brickearth (Ospringe, Pit 2). **d** Discontinuous, fine, white, horizontal calcified rootlets forming a distinct ‘root mat’ horizon within the middle part of the calcareous brickearth (note the lack of rootlets seen below this zone)

interpret the variation in geotechnical properties in relation to the composition and fabric development of the brickearth. These mineralogical studies and their influence on engineering behaviour are described in this paper.

### Description of the study sites

Investigations focused on the north Kent brickearth sequences at Ospringe near Faversham and Pegwell Bay,

**Table 1** Lithological description of the Brickearth sequence at Ospringe Pit 1

| Unit                              | Depth (m) | Description   |
|-----------------------------------|-----------|---|
| Topsoil                           | 0–0.4     | Grey brown silty clay, penetrated root channels containing fibrous remnants of recent vegetation (grasses). Modern roots penetrate vertically from the surface to c. 2.5 m. Base of topsoil is sharply defined by a thin (<0.05 m) layer of fine to medium (5–20 mm) flint, chalk and brick gravel. Rare fragments of knapped or tooled flint artefacts found at this level. Neolithic flint flakes have also been recorded from silty hillwash deposits resting on a palaeosol surface on 'non-calcareous' brickearth at Pegwell Bay (Weir et al. 1971). The top surface of the brickearth at Ospringe may be of similar age   |
| Upper 'non-calcareous' brickearth | 0.4–2.1   | Well-drained, yellowish brown, firm clay/silt with close-spaced prismatic fissuring. Undulating base of the unit is very sharp, and is differentiated from underlying calcareous brickearth by a marked colour contrast across this interface (Fig. 3a) that varies between about 2.0–2.5 m in depth across the site. Rare, angular clasts of fine to medium flint gravel (2–10 mm) occur scattered within the basal 40 mm of the unit. Abundant, sub-vertical root channels, mostly between 2–10 mm diameter, penetrate from the top to the base of the unit, continuing just into the top of the underlying calcareous brickearth (Fig. 2). These are lined or filled by porous and fibrous carbonaceous relict root material, or spongy, relict, woody roots up to 3 mm diameter. Many root channels are open and can contain small (<8 mm) fragments of chalk and flint (and near the top, red brick) derived from the overlying topsoil. Although the matrix of the clay/silt is essentially non-calcareous, many of these hollow root channels in the lower 0.5 m of the unit are lined or partially filled by white, powdery and porous, fine needle-fibre calcite (similar to that more extensively developed in the 'non-calcareous' brickearth at Pegwell Bay, see Fig. 3b). The carbonaceous root channels are truncated by the very sharp base of the topsoil but may be exploited by modern grass and cereal crop roots. The old 'carbonaceous' root channels reflect vegetation growth on the surface of the upper brickearth, whilst modern roots derive from the present topsoil  |
| Lower calcareous brickearth       | 2.1–3.0   | Well-drained, pale yellowish brown to yellowish grey, firm calcareous clay/silt with occasional scattered angular fine to medium flint gravel, up to 10 mm diameter. Very fine (1–2 mm thick) clay laminae occur below about 2.35 m. Three distinct zones can be distinguished: <p><i>2.1–2.5 m Vertical 'rhizolithic calcrete' zone:</i> dominated by abundant vertical/sub-vertical white, calcified rootlets. In contrast to the needle-fibre calcite lining root channels in the overlying 'non-calcareous' brickearth, the calcite cementing these calcified root channels is relatively dense and non-porous. Small white nodules of calcite 1–5 mm diameter are developed in clusters and patches in the brickearth around rootlets between 2.1 and 2.3 m depth. The calcified root structures, typically between 1 and 5 mm diameter and mostly up to 0.25 m in length, are best developed in the upper 0.4 m of the calcareous brickearth unit. Below 2.3 m, the abundance of vertical calcified rootlets and calcite nodules decreases significantly. However, occasional larger calcified root structures up to 10 mm diameter and over 1 m in length penetrate the underlying Thanet Formation. Within the calcareous brickearth, the vertical rootlets are mostly undisrupted but are truncated or 'planed-off' at the interface with the overlying 'non-calcareous' brickearth (Fig. 3c). This zone appears to be laterally extensive and occurs throughout the site</p> <p><i>2.5–2.75 m Horizontal 'rhizolithic calcrete' zone:</i> dominated by a meshwork of locally abundant, very fine, white, calcified horizontal rootlets or root channels, typically about 1 mm diameter, forming a 'calcified root mat.' Rare, thicker (up to 5 mm diameter) subhorizontal calcified roots may occasionally be present. The individual rootlets are usually discontinuous or broken up (Fig. 3d), and the layer is penetrated and cut through by isolated, large, vertical calcified roots from above. Thin (5–10 mm) and discontinuous lenses of clay are sometimes present. This horizontal 'root mat' horizon appears to be of limited lateral extent and was not observed in Pit 2. However, a discrete horizon of rounded to irregular calcrete nodules or calcite concretions up to 20 mm diameter were recorded at a similar depth from Pit 2, at 0.6–0.7 m below the top of the calcareous brickearth. The nodules display branched growth parallel to bedding, and locally coalesce to form a weak and discontinuous 'rubbly' layer. The vertical calcified roots largely terminate at, or merge with, this nodular calcrete layer, with only a few larger structures penetrating deeper</p> <p><i>2.35–3.0 m Cryoturbated zone</i> cryoturbated sequence, with contorted, non-systematically folded and disrupted fine (1 mm scale) clay laminae. These deformed fabrics are overprinted and cut by the undistorted later horizontal and vertical rhizolithic calcrete. Rare sand-filled wedge-like fissures (ice-wedges) are also observed in Pit 2</p> |

**Table 1** continued

| Unit                             | Depth (m)             | Description  |
|----------------------------------|-----------------------|--|
| Ferruginous mottled silty gravel | 3.0–3.2               | Lower part of calcareous brickearth grades into c. 0.15–0.2 m of gravelly silt/silty gravel, comprising sub-rounded to angular fine to medium (5–10 mm) flint gravel clasts in an inhomogeneous matrix varying from reddish brown, ‘non-calcareous’ silty fine sand (similar to the sand facies in underlying Thanet Formation) to calcareous yellowish brown silt (similar to the overlying brickearth), which has been disturbed to some extent by cryoturbation. The silty gravel is stained by orange-red ferruginous mottles forming ovoid to irregular patches up to 0.1 m diameter. This unit rests with a sharp base on the underlying Thanet Formation, and a slightly irregular, possibly eroded top |
| Thanet formation (sand facies)   | 3.2–3.8               | Light reddish brown, dense silty fine sand with occasional small angular flint pebbles forming the top of the Palaeocene Thanet Formation. This sand is cut by rare large vertical calcified root structures that penetrate from the overlying calcareous brickearth   |
| Thanet formation (Bullhead Bed)  | 3.8–4.7 (base of pit) | Well-drained, light red-brown, poorly sorted gravel with sub-rounded cobbles of flint in a matrix of clay/silt to fine sand. Very rare, sub-vertical calcified root structures (rhizolithic calcrete) or calcite-cemented root channels (up to 6 mm diameter) can be traced down into the top 0.2 m this unit from the overlying calcareous brickearth   |

supplemented by limited observations made on a small number of samples of calcareous brickearth samples collected from southeast Essex, West Sussex and Paignton (south Devon) (Fig. 1). The Ospringe and Pegwell Bay sites are described below. It should be noted that in the descriptions provided, distinction is made between upper *non-calcareous* and lower *calcareous* brickearths. Despite being described as ‘non-calcareous,’ our petrographical analyses showed that the presence of primary detrital carbonate grains (including chalk and foraminifera fragments in a micritic calcite matrix) are present in the upper brickearth, but as accessory components only. This is in marked contrast to the much more dominant calcareous component of the lower brickearths.

#### Ospringe brickworks

The Ospringe brickearth sequence was examined in a brickworks borrow area, just southeast of Faversham in north Kent. The site is on arable farmland situated at around +27 m OD on the northeast slope of a chalk coombe that runs into Oare Creek (a tributary of the River Swale). The 1:50,000 scale geological map (Faversham, Sheet 273) shows the brick pit is developed in Head Brickearth, overlying the Thanet Formation (comprising very dense, light yellow–brown silty or clayey fine sand with basal clayey or silty sand and gravel) or the Bullhead Bed (flint cobble deposit), or the White Chalk Subgroup. A brickearth sequence, approximately 2.8 m thick, was examined and sampled in detail in a temporary pit (Ospringe Pit 1: National Grid Reference TQ 599700 161164) exca-

vated by mechanical digger to a depth of 4.7 m. Subsequent samples were collected for optically stimulated luminescence (OSL) dating analysis from a second pit some 10 m distant from Pit 1 (Ospringe Pit 2; National Grid Reference TQ 599704 161251). The lithological sequence (Ospringe Pit 1) is summarised in Figs. 2, 3 and described in detail in Table 1.

#### Pegwell Bay

Brickearth deposits are exposed in the sea cliffs on the north side of Pegwell Bay, between Ramsgate and Pegwell, where they overlie silty calcareous clays and fine sands of Thanet Formation strata of variable thickness resting on the frost-shattered Upper Chalk (Pitcher et al. 1954; Kerney 1965; Weir et al. 1971; Catt 1977; Antoine et al. 2003). Soliflucted channel sands with lenses of gravel also occur intermittently cut into the Thanet Formation, and along with the underlying Chalk and Thanet Formation are cryogenically disturbed and convoluted (Kerney 1965).

A 1.6-m sequence of brickearth was examined from a bench section cut into well-exposed cliff-top sediments, sited just above the disused beach access tunnel near Cliffsend (National Grid Reference TR 635586 164364). The base of the brickearth was not exposed in the bench, and therefore its relationship with the underlying Thanet Formation was not seen. The section displays features broadly similar to the Ospringe site with a discrete upper ‘non-calcareous’ brickearth and a lower calcareous brickearth. The sequence is summarised in Fig. 2 and described in detail in Table 2.

**Table 2** Lithological description of the Brickearth sequence at Cliffend, Pegwell Bay

| Unit                              | Depth (m)                 | Description  |
|-----------------------------------|---------------------------|--|
| Topsoil                           | 0–0.3                     | Well-drained, dark grey-brown, organic-rich silty clay, containing abundant scattered small angular clasts of fine to medium flint gravel (3–10 mm). The site is wooded with hazel and birch, and a dense, modern root mat of sub-horizontal and vertical woody roots up to 50 mm in diameter is developed within the topsoil. Modern vertical tree roots penetrate the underlying brickearth to >1.6 m, commonly exploiting older carbonaceous root channels  |
| Upper 'non-calcareous' brickearth | 0.3–1.2                   | Two sub-units may be recognised:<br>0.3–0.6 m <i>Palaeosol</i> Well-drained, firm or compact, fissured reddish brown to brown clay/silt, markedly disturbed by roots and burrowing animals, and cut by numerous close-spaced hairline fissures. Abundant old, open root channels (up to 10 mm in diameter) are present, containing partially decomposed, carbonaceous and fibrous root remnants. These root channels abruptly terminate at the interface with the overlying topsoil. Calcite is absent in both the soil matrix and the root channels. The base is diffuse, irregular and gradational into the underlying more coherent and compact 'non-calcareous' brickearth<br>0.6–1.2 m <i>Firm 'non-calcareous' brickearth</i> Medium to light brown silt/clay, exhibiting a decrease in disruption and fissuring with depth. Abundant vertical root channels (up to 10 mm diameter) are present containing carbonaceous rootlets, relict partially decomposed fibrous root material and white, powdery, friable, and needle-fibre calcite. Needle-fibre calcite also locally permeates the adjacent brickearth matrix for up to 20 mm along lateral root hair channels and irregular fissures in the soil (Fig. 3b) but the soil matrix is otherwise non-calcareous. Needle-fibre calcite disappears as the brickearth grades into the palaeosol horizon above. Modern roots also penetrate this brickearth but are less abundant than in the overlying 'disrupted brickearth' or palaeosol horizon. Vertical burrows (up to 12 mm diameter) partially filled with pale grey-brown clay, occur in the lower part of the unit and penetrate into the top of the underlying calcareous brickearth. Cavities in these burrows are lined by white needle-fibre calcite. As at Ospringe, the base of the unit has a very sharp, slightly undulating base, which is differentiated from the underlying calcareous brickearth by a marked colour difference (Fig. 3b) |
| Lower calcareous brickearth       | 1.2–1.6 (base of section) | Well-drained, firm pale yellowish brown to yellowish grey, calcareous silt. A zone of rhizolithic and fine nodular calcrete is developed in the upper 9 cm of the unit, with abundant vertical calcified rootlets, 10–20 mm long and 0.5–1 mm diameter, with finer lateral calcified rootlets and root hairs. Small nodules of calcite (1–3 mm diameter) are common and tend to be clustered around the calcified roots. Occasional larger calcified roots up to 5 mm diameter penetrate to >1.6 m depth. The calcified roots are characterised by a concentric, laminated micritic calcite fill. They are truncated and planed-off at the contact with the overlying 'non-calcareous' brickearth, clearly indicating that this lithological boundary is an erosional surface. The fine nodular calcrete is absent below 1.3 m. However, a discrete layer of coarser calcite concretions or calcrete nodules occurs at a depth of 1.60 m, at the base of the exposed profile. These nodules are 5–40 mm in diameter, rounded to irregular and elongated and branched parallel to the bedding. The larger vertical calcified roots appear to terminate at, or merge with, the nodules in this horizon   |

## Samples and analytical methods

### Bulk mineralogical characterization

Whole-soil and clay mineralogy of the brickearths were determined by X-ray diffraction (XRD) analysis of bulk soil and <2 µm orientated fraction material, respectively. In addition, XRD analysis was undertaken on small amounts of white fibrous/powdery mineral coatings lining root channels and fissures following careful separation and preparation. XRD analyses were conducted using a Philips PW1700 series diffractometer fitted with a cobalt-target tube and operated at 45 kV and 40 mA. Errors for the quoted mineral concentrations are around ±5 % accuracy for quartz, calcite, hematite and dolomite. Larger errors are possible for 'mica,' chlorite, smectite, kaolinite, amphibole

and feldspar concentrations. The relative proportions of clay minerals present in the <2 µm fractions were determined by modelling of their XRD profiles using Newmod-for-Windows™ software (Reynolds and Reynolds 1996). The procedure followed for modelling the individual clay mineral species established *mineral reference intensities* that were used for quantitative standardisation following the method outlined in Moore and Reynolds (1997).

Total (internal and external) mineral surface areas were determined by the ethylene glycol monoethyl ether (EGME) sorption under vacuum method (Carter et al. 1965). The surface area of a sample can provide a useful estimate of its smectite content since smectite has a high surface area (800 m<sup>2</sup>/g), whereas other clay minerals and quartz have lower surface areas typically <100 and 1 m<sup>2</sup>/g, respectively.



## Petrographical analysis

Undisturbed blocks of soil were collected for petrographical analysis using  $100 \times 50$  mm thin-walled aluminium sampling boxes (Kubiëna tins). These were inserted into the face of the soil profile by cutting the soil from around the margins of the tin with a knife, whilst gently pressing the tin into the exposed soil face. Once emplaced, the soil tin containing the intact soil block was carefully excavated from the soil, trimmed and tightly sealed. Polished thin sections were prepared from these preserved samples following air-drying at room temperature and stabilization by vacuum impregnation with epoxy-resin. A blue dye was added to the epoxy resin to enable any porosity to be readily identified during examination in transmitted light under the optical petrological microscope. Optical cold-cathode cathodoluminescence microscopy (CL) was used to examine calcite cement fabrics. High-resolution mineralogical and petrographical observations were undertaken by backscattered scanning electron microscopy (BSEM) using a LEO435VP variable pressure scanning electron microscope (SEM). The SEM instrument was operated using a 10–20 kV electron beam and beam currents of 300–600 pA, and under low vacuum (0.3 torr), enabling the thin sections to be imaged without the need for carbon coating required in conventional (high-vacuum) SEM analysis (Large et al. 2001).

Grain fabrics and pore morphologies were also examined by SEM using secondary electron imaging of freshly broken surfaces of intact brickearth. In addition, SEM observations were made of disaggregated silt and sand grain surfaces, following cleaning and removal of clay/iron oxide coatings by ultrasonic dispersion of the sediment samples in deionised water. These samples were vacuum-coated with carbon for high-resolution, conventional high-vacuum SEM observation. SEM images were recorded using an electron beam accelerating voltage of 10–20 kV and beam currents of 50–200 pA.

Mineral identification was aided by qualitative energy-dispersive X-ray microanalyses (EDXA) acquired during SEM and BSEM imaging using an Oxford Instruments ISIS300 EDXA system with a Si–Li X-ray detector.

## Optically-stimulated luminescence dating

A limited dating study was made to try to establish the age relationships between the ‘non-calcareous’ and calcareous brickearths horizons at Ospringe and Pegwell Bay (two samples from each site). Large  $100 \times 100$  mm aluminium Kubiëna boxes were used to collect undisturbed samples of loessic brickearth from freshly cleaned soil faces just above and just below the interface between the two brickearth

horizons. The sample tins were capped with tightly fitting aluminium lids and sealed with black adhesive tape to keep out light. Horizontal holes were augered into the soil face at each sampling point and a gamma spectrometer probe inserted to record the in situ gamma radiation dose from surrounding soil mass. The samples were analysed by optically stimulated luminescence (OSL) technique at the University of Nottingham. OSL analyses were performed on the 4–11  $\mu\text{m}$  fine silt fraction (both polyminerals and quartz extracts) and on the 35–50  $\mu\text{m}$  modal quartz fraction after treatment to remove feldspars. Full details of the OSL dating study of the brickearths are described by Clarke et al. (2007).

## General mineralogical characteristics

Whole-soil, clay mineral data, total clay content and EGME surface area information for the brickearth from Ospringe and Pegwell Bay are presented in Table 3. The whole-soil mineralogy of the brickearth is broadly similar at both sites, comprising: 50–75 % quartz; 3–10 % K-feldspar; 2–9 % plagioclase (albitic); 9–17 % ‘mica’ (including muscovite, biotite and illite, undifferentiated by whole-soil XRD); minor kaolinite and smectite. Traces of chlorite and hematite were also detected in the upper part of the Pegwell Bay sequence, and were observed in thin sections from both sites. In addition, traces of amphibole were found in some samples from Ospringe, and rutile was identified as a trace mineral at both sites. A very small amount of halite was detected in samples of the lower (calcareous) brickearth at Pegwell Bay. This is a residue from sea-spray as this is a cliff-top site. The  $<2 \mu\text{m}$  ‘clay fraction’ XRD data, together with total clay content values determined from grain size analysis (Table 3), indicate that clay minerals and the poorly-ordered smectite in particular may be underestimated by the whole-soil XRD analyses. However, the  $<2 \mu\text{m}$  fraction XRD data does not take into account the clay-sized quartz that is present in these loessic sediments, which will reduce the actual clay mineral concentration. Furthermore, the modelling used to quantify the whole soil mineralogy does not adequately handle the turbostratic crystal structure of smectite. The clay mineralogy is dominated by smectite (38–84 %), with subordinate illite (5–34 %) and kaolinite (9–27 %) and minor chlorite (0–10 %). In the case of the Ospringe site, these data suggest that smectite may contribute between 6 and 21 % of the total sediment mass (assuming no  $<2 \mu\text{m}$  quartz is present), which is consistent with the moderately high EGME surface area values observed (Table 3). Brickearths from Pegwell Bay have lower surface area values than comparable sediments at Ospringe, which might be indicative of a slightly coarser grain-size.

**Table 3** Summary XRD mineralogy, EGME surface area and clay content (determined from particle size) data for Osprunge and Pegwell Bay

| Site             | Depth (m)             | Lithology             | Sample no. | Whole-soil XRD (%) |          |           |        |          |          |            |              |        |          | <2 µm clay XRD (%) |        |          |           |      | Clay content (%) | Surface area (m <sup>2</sup> /g) |
|------------------|-----------------------|-----------------------|------------|--------------------|----------|-----------|--------|----------|----------|------------|--------------|--------|----------|--------------------|--------|----------|-----------|------|------------------|----------------------------------|
|                  |                       |                       |            | Calcite            | Dolomite | Kaolinite | 'Mica' | Smectite | Chlorite | K-feldspar | Albite (low) | Quartz | Hematite | Smectite           | Illite | Chlorite | Kaolinite |      |                  |                                  |
| Osprunge [Pit 1] | 0.60                  | Non-calc. brickearth  | J261       | nd                 | 0.5      | 6.3       | 12.6   | 0.7      | nd       | 6.9        | 8.7          | 64.3   | nd       | 38                 | 34     | 10       | 19        | 17.5 | 104              |                                  |
|                  | 0.80                  | Non-calc. brickearth  | J262       | nd                 | 0.9      | 5.1       | 13.3   | 0.7      | nd       | 10.2       | 6.2          | 63.6   | nd       | 51                 | 20     | 9        | 20        | 29.8 | 102              |                                  |
|                  | 1.10                  | Non-calc. brickearth  | J263       | nd                 | 0.5      | 4.5       | 15.5   | 1.1      | nd       | 7.5        | 6.8          | 64.1   | nd       | 47                 | 25     | 8        | 21        | 27.3 | 109              |                                  |
|                  | 1.30                  | Non-calc. brickearth  | J264       | nd                 | 0.5      | 3.2       | 12.8   | 1.7      | nd       | 6.3        | 4.2          | 71.3   | nd       | 57                 | 16     | nd       | 27        | 11.6 | 108              |                                  |
|                  | 1.50                  | Non-calc. brickearth  | J265       | nd                 | 0.7      | 4.9       | 12.9   | 1.5      | nd       | 6.2        | 6.4          | 67.4   | nd       | 61                 | 20     | 6        | 14        | 34.5 | 114              |                                  |
|                  | 1.85                  | Non-calc. brickearth  | J266       | nd                 | 0.9      | 4.9       | 14.4   | 1.6      | nd       | 5.1        | 6.8          | 66.3   | nd       | 48                 | 21     | 11       | 20        | 30.2 | 105              |                                  |
|                  | 2.00                  | Non-calc. brickearth  | J267       | nd                 | 1.0      | 5.1       | 12.9   | 1.3      | nd       | 5.4        | 7.2          | 67.1   | nd       | 66                 | 16     | 6        | 13        | 38.9 | 97               |                                  |
|                  | 2.20                  | Calcareous brickearth | J268       | 12.8               | 4.2      | 4.7       | 13.8   | 1.0      | nd       | 5.0        | 5.6          | 52.9   | nd       | 45                 | 30     | 7        | 18        | 17.3 | 74               |                                  |
|                  | 2.40                  | Calcareous brickearth | J269       | 8.7                | 4.0      | 4.5       | 14.3   | 1.5      | nd       | 5.3        | 6.0          | 55.7   | nd       | 63                 | 17     | -        | 20        | 14.9 | 61               |                                  |
|                  | 2.70                  | Calcareous brickearth | J270       | 8.0                | 2.2      | 3.2       | 11.6   | 1.5      | nd       | 5.7        | 4.8          | 63.0   | nd       | 52                 | 25     | 7        | 16        | 17.5 | 79               |                                  |
|                  | 2.90                  | Calcareous brickearth | J271       | 4.0                | 1.8      | 5.2       | 14.7   | 1.2      | nd       | 5.8        | 3.6          | 63.7   | nd       | 73                 | 14     | 4        | 9         | 18.4 | 89               |                                  |
|                  | 3.10                  | Ferrug. silty gravel  | J272       | <0.5               | 1.3      | 4.4       | 16.9   | 2.2      | nd       | 7.3        | 4.8          | 62.8   | nd       | 68                 | 12     | 6        | 14        | 21.6 | 116              |                                  |
|                  | 3.50                  | Thanet Formation      | J273       | 0.5                | 0.6      | 5.1       | 16.1   | 2.6      | nd       | 6.9        | 5.1          | 63.1   | nd       | 82                 | 6      | 4        | 8         | 18.4 | 120              |                                  |
|                  | ~0.75                 | Non-calc. brickearth  | G355       | nd                 | nd       | 2.5       | 11.0   | 1.5      | <0.5     | 6.1        | 5.8          | 72.5   | <0.5     | 84                 | 5      | 4        | 7         | na   | 64               |                                  |
| ~0.75            | Non-calc. brickearth  | G370                  | 0.9        | nd                 | 10.9     | 15.7      | 1.4    | <0.5     | 2.6      | 5.6        | 62.2         | <0.5   | 40       | 30                 | 9      | 21       | na        | na   |                  |                                  |
| 1.40             | Calcareous brickearth | J274                  | 12.5       | 0.4                | 1.9      | 9.4       | 0.6    | nd       | 7.0      | 2.8        | 65.1         | nd     | 57       | 24                 | 6      | 14       | na        | 54   |                  |                                  |
| 1.60             | Calcareous brickearth | J275                  | 14.0       | 1.4                | 2.1      | 10.7      | 1.1    | nd       | 4.2      | 3.8        | 62.6         | nd     | 50       | 30                 | 7      | 12       | na        | 53   |                  |                                  |
| 1.70             | Calcareous brickearth | J276                  | 15.4       | 4.0                | 3.5      | 12.9      | 1.1    | nd       | 5.9      | 5.6        | 51.6         | nd     | 46       | 29                 | 7      | 18       | na        | 55   |                  |                                  |
| 1.90             | Calcareous brickearth | J277                  | 11.2       | 0.9                | <0.5     | 9.6       | 1.3    | nd       | 2.8      | 1.6        | 72.2         | nd     | 65       | 18                 | 5      | 12       | na        | 48   |                  |                                  |

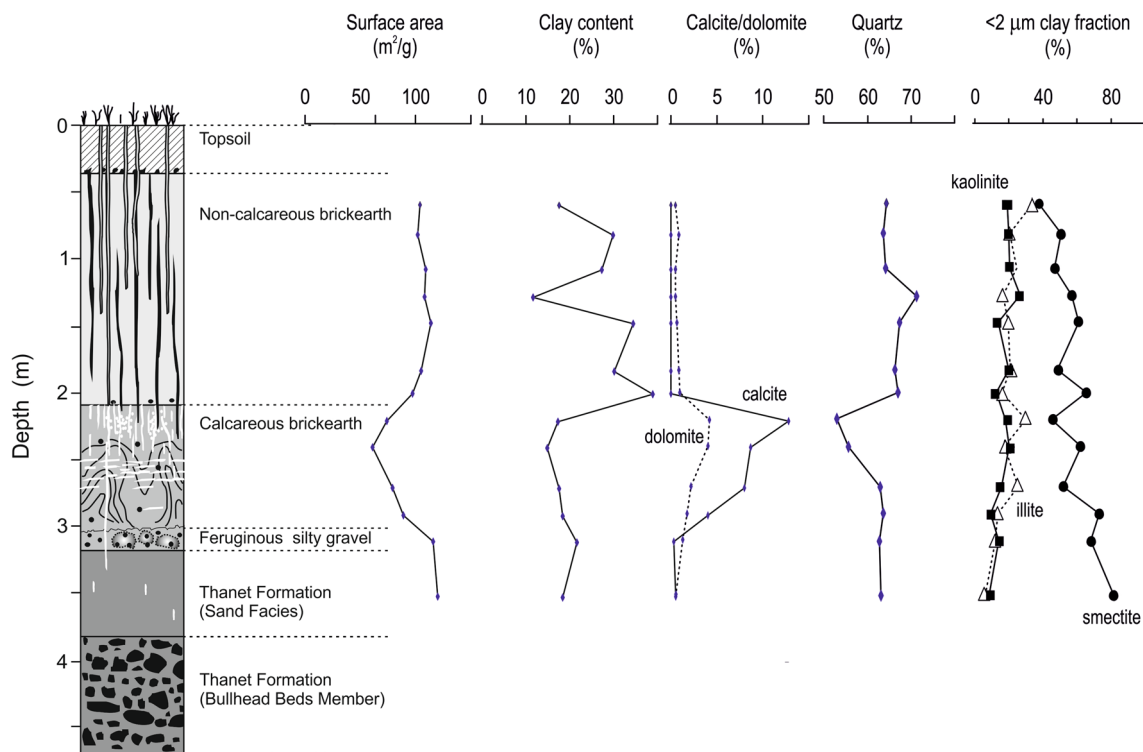


**Fig. 4** Mineralogical variation with depth through the Ospringe brickearth profile (Pit 1)

Significant variations in mineralogy with depth are observed at both sites, particularly for carbonate minerals (Table 3). The principal variations in the Ospringe sequence are summarised in Fig. 4. The lower brickearth unit is characterised by significant calcite (calcareous brickearth). Calcite concentration (which is <0.5 % in the Thanet Formation and overlying ferruginous silty gravel) progressively increases from 4 % at the base of the brickearth sequence to a peak of about 13 % corresponding to the maximum development of the ‘vertical rhizolithic calcrete zone’ (2.1–2.5 m) at the top of the lower brickearth unit (Figs. 2, 4). However, the calcite content falls sharply from its peak value (13 %) at the top of the calcareous brickearth to 0 % in the overlying (‘non-calcareous’) brickearth unit. The disappearance of calcite coincides precisely with the ‘planed-off’ eroded top of the rhizolithic calcrete zone (Figs. 2, 4). Dolomite is also present and follows a similar trend to calcite, rising from 0.6 % in the Thanet Formation to about 4 % at the top of the calcareous brickearth, before falling sharply to <1 % in the overlying ‘non-calcareous’ brickearth. However, XRD analyses also indicate that trace amounts of dolomite persist throughout the upper brickearth unit. Quartz, and clay content distributions display an antithetic relationship to that of calcite (Fig. 4), representing the ‘dilution’ effect of the calcite. Surface area broadly follows the clay content, and will be influenced by the abundance of high surface

area clay minerals such as smectite (Fig. 4). Similar mineralogical differences are observed in the Pegwell Bay brickearth, with calcite and dolomite present in the lower part of the sequence, coinciding with the development of rhizolithic and nodular calcrete but absent (apart from a trace of calcite) in the overlying ‘non-calcareous’ brickearth, their disappearance coinciding with the interface between the upper and lower brickearth units.

If allowance is made for the dilution effect due to the development of the carbonate minerals, then an overall trend of increasing clay content and quartz is observed from the base to the top of the brickearth sequence at Ospringe (Fig. 4). Within the <2 µm fraction, there is also a slight progressive increase upward through the brickearth profile for illite and, more subtly, kaolinite. In contrast, smectite shows a twofold decrease in concentration from the base to the top of the brickearth sequence. Intermittent large decreases in clay content are indicated at 1.3 and 0.6 m in the upper brickearth (Fig. 4) but are not reflected in the trends for quartz, clay mineralogy or surface area. Petrographic observations show that these intervals coincide with an increase in silt- and fine sand-size components (compare Fig. 5a, b). Furthermore, patchy fine or amorphous iron oxide (or oxyhydroxide) cement (Fig. 5a) is more abundantly developed in these coarser silt horizons and towards the top of the ‘non-calcareous’ brickearth. This cement inhibits

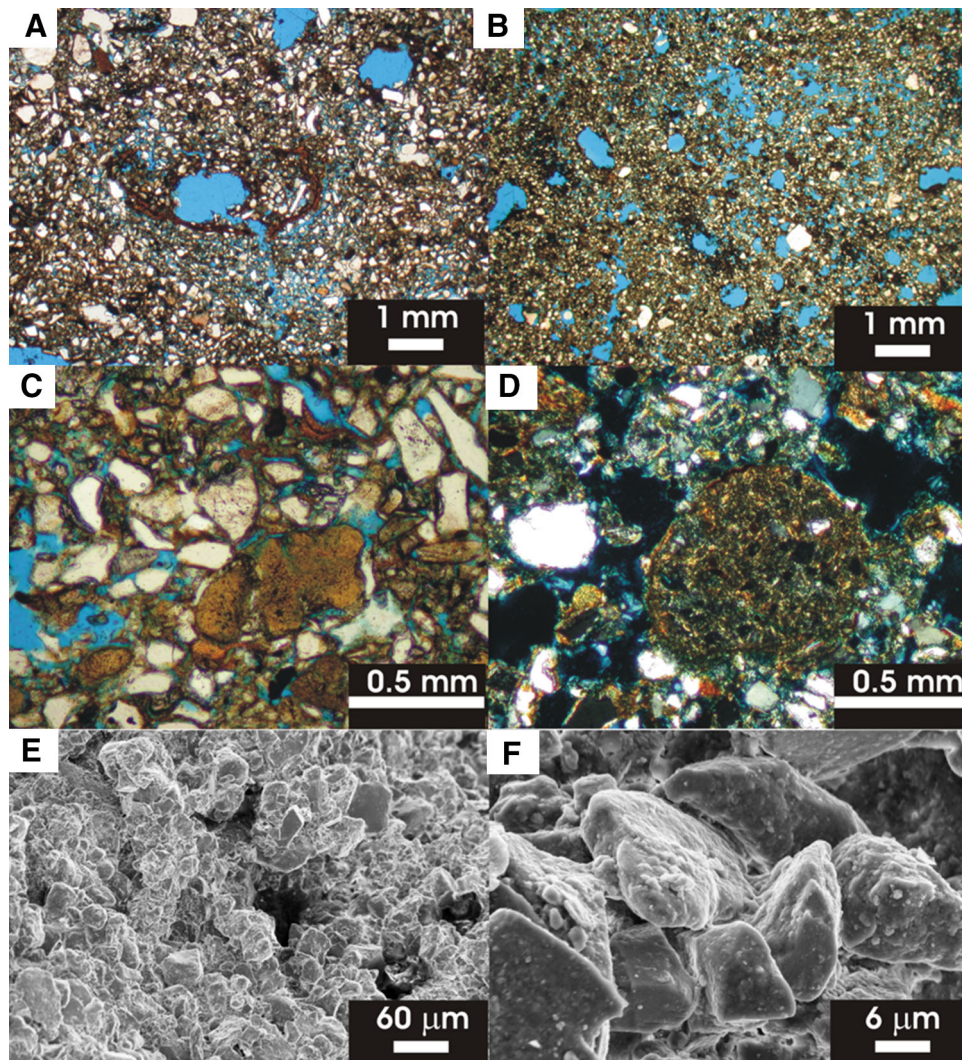


**Fig. 5** **a** Thin section photomicrograph (transmitted light) showing close-packed angular silt and sub-rounded fine quartz sand with a matrix of iron-oxide (opaque) impregnated clay, with localised areas of more open-packed silt fabric (highlighted by the blue-dyed epoxy resin impregnation of intergranular porosity). Iron oxide impregnated the clay (ferriargillan) voids after the root hairs, and wisps of iron oxide-stained clay (plasmic clay) can be seen where clay-lined root channels have been disrupted or collapsed. 'Non-calcareous' brickearth, 1.28–1.37 m, Ospringe Pit 1. **b** Thin section photomicrograph (transmitted light) of very fine silt and clay with occasional grains of coarse silt and fine quartz sand, containing abundant channel-like voids after root hairs, locally surrounded by haloes of opaque iron oxide. 'Non-calcareous' brickearth, 1.70–1.79 m, Ospringe Pit 1. **c** Thin section photomicrograph (transmitted light) showing well-

rounded brown (oxidized) glauconite sand grains (centre) in a compact quartz-dominated silt matrix. 'Non-calcareous' brickearth, 1.28–1.37 m, Ospringe Pit 1. **d** Thin section photomicrograph (crossed polarised light) showing a well-rounded lithic clast (centre) replaced by birefringent smectite (possibly altered volcanic glass). 'Non-calcareous' brickearth, 1.70–1.79 m, Ospringe Pit 1. **e** SEM photomicrograph showing dominantly compact close-packed silt grain fabric, and large voids that represent root-hair channels. 'Non-calcareous' brickearth, 1.0 m, Ospringe Pit 1. **f** SEM photomicrograph showing detail of compact close-packed fabric of interlocking angular silt grains. The silt grains are completely coated with a gelatinous film of clay. 'Non-calcareous' brickearth, 1.0 m, Ospringe Pit 1

dispersion and desegregation of fine silt and clay during particle size analysis, giving rise to anomalous and apparently low clay contents. The silt- and sand-sized material is dominated by angular quartz with minor K-feldspar, albitised plagioclase, and chert fragments. However, the brickearth also contains scattered well-rounded and often oxidized glauconite grains (Fig. 5c),

and highly altered and ferruginous smectite-replaced clasts (Fig. 5d) that probably represent altered fragments of volcanic glass. These are more common in the lower calcareous brickearth and in the sporadic coarser sandier intervals in the overlying 'non-calcareous' brickearth. Well-rounded detrital calcareous lithic grains are occasionally observed in both the upper and lower brickearth

units. These comprise microporous micrite (chalk) often containing foraminifera tests. No evidence is seen in thin sections for dissolution of the carbonate clasts in either brickearth unit. Similar features are seen at Pegwell Bay.

Erosion and re-working of the underlying Thanet Formation is the most likely source of smectite, glauconite, altered volcanic glass and chert fragments found in the north Kent brickearths (cf. Knox 1979). The rare detrital carbonate grains may also be reworked from these Tertiary strata, or possibly derived directly from the chalk. The upward decrease of these components observed in the brickearth sequence indicates that mixing with sediment derived locally from the Thanet Formation became less important with time.

### Brickearth fabric and post-depositional (diagenetic) modification

#### 'Non-calcareous' brickearth

'Non-calcareous' brickearth at Ospringe and Pegwell Bay sites is characterised by a dominantly compact grain-supported fabric of close-packed, angular grains of quartz silt and fine sand, with interstitial clay and fine silt (Fig. 5e, f). The silt/sand quartz grains are typically interlocked and a gelatinous skin of smectite-illite-kaolinite clay completely coats the grains on which finer quartz particles adhere (Fig. 5f). The clay forms a meniscus film between the quartz grains in close contact and partially fills the intergranular spaces (Fig. 6a). Only relatively rarely does the clay form discrete 'bridges' between silt grains that are not in direct physical contact. The fabric is locally heterogeneous, and contains irregularly distributed 'domains' of silt that possess a more open grain framework with significant intergranular porosity (Fig. 5a, b). Grain-bridging clay fabrics are better developed in these domains but they account for only a very small proportion of the soil volume. Traces of weakly developed ped fabric can sometimes be observed in the 'non-calcareous' brickearth. The peds consist of diffuse, round pellet-like aggregates (0.3–1 mm diameter) of compact silt with a clay matrix; they are often defined in thin section by weakly iron oxide-stained rims (just discernable in Fig. 5a, b). The peds are close-packed, with more open-packed silt filling the residual space between the peds, although this fabric has largely been destroyed and homogenised through bioturbation by roots and root hairs.

The basal 5–10 cm of the unit is finely laminated; comprising 0.2–0.6 mm laminae of well-sorted fine sand and medium to coarse silt, with scattered grains of well-rounded and angular medium quartz sand. Lamination has been disrupted by fine root channels and also many of these

channels are partially collapsed, leaving localised 'domains' of less packed sand and silt up to 0.5–1 mm across. This fine lamination suggests that the lower part of the 'non-calcareous' brickearth may possibly have been deposited in water and/or reworked by water.

The 'non-calcareous' brickearth fabric has been extensively modified by the activity of plant roots. Significant macroporosity is present in the form of fine channel-like voids ranging from 0.1 to 1 mm in diameter (Fig. 5a, b, e), representing channels left after the decomposition of rootlets and root hairs. These are particularly abundant in the upper 1 m of sediment but are present throughout the brickearth sequence. The fibrous remains of decomposed roots can still be observed in some of these channels. Localised collapse of root channels and infilling with loose silt and clay accounts for some of the fabric heterogeneity described above. Growth of the root hairs compacted the silt adjacent to the walls of the channel for a distance of several grain diameters. Infiltrated (illuvial) clay forms finely laminated films that line the channels, binding the silt in the walls. In addition, fine secondary ferric iron oxide or oxyhydroxide precipitated within these clay films ('ferriargillans') and in the silt matrix adjacent to many of the root channels. Amorphous iron oxide or goethite may cement and further strengthen the root channel walls, and help bond the silt fabric. Secondary iron oxide formation is most abundant towards the upper part of the 'non-calcareous' brickearth, particularly in the palaeosol horizon above 0.62 m (Fig. 2) at the Pegwell Bay site. Disrupted and deformed wispy ('plasmic') fragments of very finely laminated ferruginous clay, similar to the ferriargillans lining the root channels and forming grain cutans (coatings), occur very sporadically. Root bioturbation may have contributed to the disruption of these clay fabrics but this could also have been caused by cryoturbation (Kemp 1985, 1987; Rose et al. 1985; Van Vliet-Lanoë 1985).

Large open carbonaceous root channels, and fine root hair channels in the lower part of 'non-calcareous' brickearth are often lined by a delicate mesh work of needle-fibre calcite (Fig. 6b): below 1.5 m at Ospringe, and below 0.62 m at Pegwell Bay (mineralogical identity confirmed by XRD of separated calcite fibres). The calcite mesh serves to reinforce and bind silt particles in the walls of the root channels, thereby helping maintain open channel porosity. Individual calcite needles are typically 15–30  $\mu\text{m}$  long (but may be up to 50  $\mu\text{m}$ ), <1  $\mu\text{m}$  wide and are smooth-sided. They resemble MA-type needle-fibre calcite related to biomineralisation inside fungal mycelia bundles (Verrecchia and Verrecchia 1994). Needle-fibre calcite is a common feature in both ancient and modern calcretes (Wright 1984; Strong et al. 1992; Becze-Deák et al. 1997; Candy 2002; Kabanov 2005). Its close association here with root channels and root remains suggests that it is also

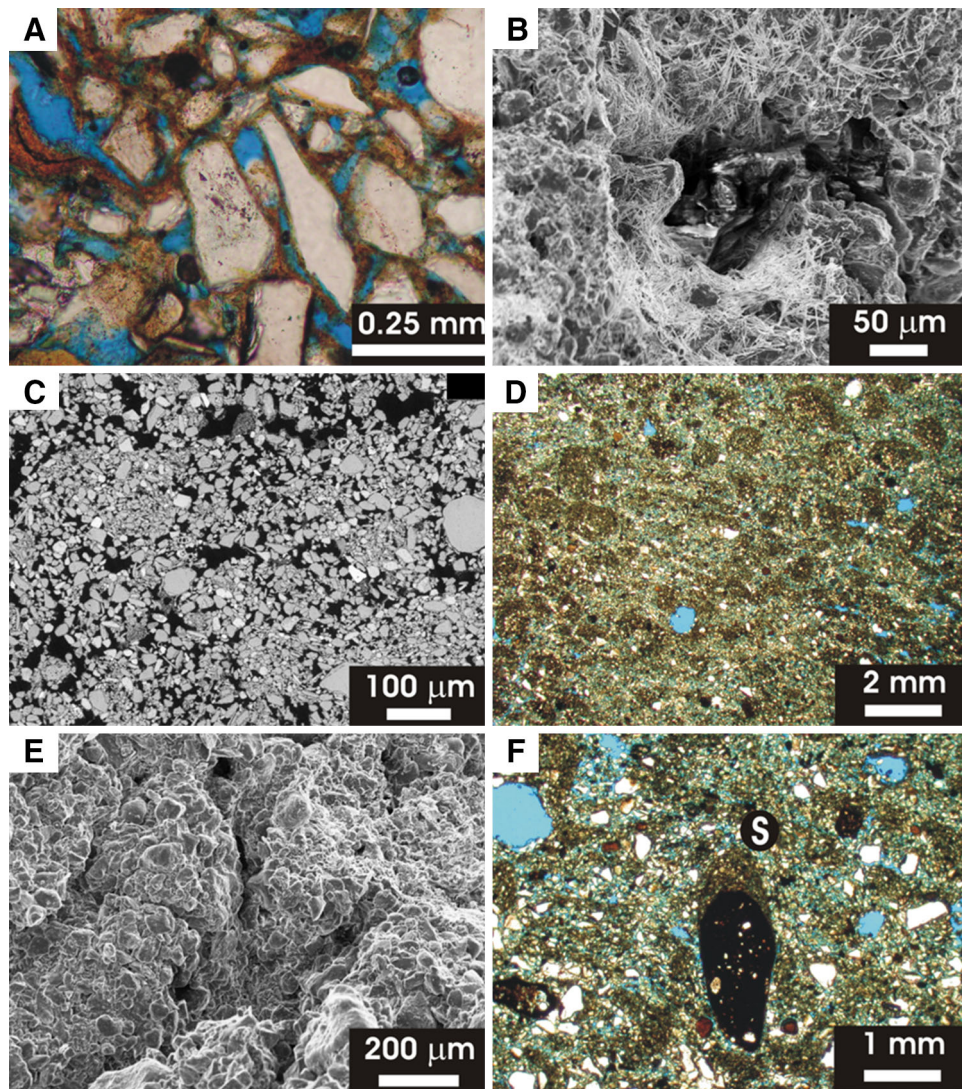


**Fig. 6** **a** Thin section photomicrograph (transmitted light) showing a thick, dark clay coating on close-packed grains of angular quartz silt. 'Non-calcareous' brickearth, 1.28–1.37 m, Ospringe Pit 1. Field of view = 0.72 mm wide. **b** SEM photomicrograph of delicate meshwork of needle-fibre calcite lining the walls of a root hair channel. Relict root material is still present (centre of channel). 'Non-calcareous' brickearth, 1.0 m, Pegwell Bay. **c** BSEM photomicrograph of polished thin section illustrating the typical fabric within calcareous brickearth, comprising a loose-packed assemblage of rounded 'pellets' or 'peds' of more compact fine silt, supported in a matrix of loose-packed silt matrix. From just beneath 'non-calcareous'/calcareous

brickearth contact, 2.06 m, Ospringe Pit 1. **d** Thin section photomicrograph (transmitted light) showing well-developed pelletised or pedified silt fabric (dark). Calcareous brickearth/mottled ferruginous silty gravel, 3.11–3.2 m, Ospringe Pit 1. **e** SEM photomicrograph of typical macroporous pelletised brickearth fabric, comprising pellets of compact silt grains (with interstitial clay) in an open-packed arrangement. Calcareous brickearth, 2.39 m, Ospringe Pit 1. **f** Thin section photomicrograph (transmitted light) showing pelletised silt fabric with fine silt/clay 'cap' (S) developed on the top of a coarse ferruginous lithic grain (opaque). Calcareous brickearth/mottled ferruginous silty gravel, 3.11–3.2 m, Ospringe Pit 1

of biogenic origin and related to saprophytic decay of organic matter (Wright 1984, 1986; Phillips and Self 1987; Kabanov 2005).

#### Calcareous brickearth

The lower calcareous brickearth is characterised by a very open framework of angular quartz silt and fine sand (Fig. 6c). However, the fabric is complex and often

displays a well-preserved pelletised structure (Fig. 6d, e), in which finer silt and clay are segregated into domains of densely-packed silt and clay to form 'rounded' pellets or peds 0.2–1 mm diameter. The peds themselves may be loosely-packed to moderately close-packed but have a very porous inter-ped matrix of coarser open-packed silt and fine sand (Fig. 6c, e). A very weak sub-horizontal platy or laminar fabric is also observed in places, comprising discontinuous thin layers of coarse silt (1–2 grain diameters

thick) separating thicker layers of pellets in the coarse silt/fine sand matrix (Fig. 6c). Grain size segregation is also occasionally seen in the formation of ‘caps’ of fine clay/silt resting on top of coarse sand and gravel clasts (Fig. 6f). Scattered silt-sized rounded pellets of compact ferruginous clay are also present. These resemble the clay-forming cutans on silt grains and lining root-hair channels, and may represent material derived from such features (sometimes referred to as ‘papulized ferriargillan’ or ‘papules’ (e.g. Rose et al. 1985; Van Vliet-Lanoë 1985). These micro-morphological fabrics are characteristic of old climate/permafrost soils, formed by repeated freeze–thaw (Kemp 1985, 1987; Rose et al. 1985; Van Vliet-Lanoë 1985) and are consistent with other evidence of cryoturbation observed in the pit profiles at Ospringe (see earlier and Fig. 2).

Silt and fine sand grains are coated with a thick (up to 5 µm) coating of illitic and smectitic clay (Fig. 7a). These cutans are thicker than those found in the ‘non-calcareous’ brickearth and a high proportion of grains are completely coated with this clay such that there is often little direct point contact between the silt grains. This clay also partially fills the intergranular pores in the more compacted pelletised (ped) silt domains (cf. ‘non-calcareous’ brickearth—cf. Fig. 5f). In the very open-packed coarser silt/fine sand filling the inter-ped domains, the clay forms very well-developed and extensive meniscus bridges between adjacent silt/sand grains. The silt/sand grains are typically dispersed and separated by 2–15 µm, with little or no direct grain-to-grain point contact, but held in place by the clay bridges that act as buttresses between the silt grains (Fig. 7b). Similar clay bridging bonds the inter-ped silt/sand to adjacent silt pellets to form a supporting skeletal fabric. High-resolution SEM observations show that mesh works of very fine needle-fibre calcite also form locally as meniscus bridges between adjacent silt/sand grains (Fig. 7c). This acicular calcite is much finer than the needle-fibre calcite lining open root cavities seen elsewhere in both the ‘non-calcareous’ and calcareous brickearths, with individual calcite fibres typically 1–10 µm long and about 0.1 µm wide. In some cases, the calcite acts as a ‘scaffold’ to support later accumulation of illuviated clay within the pores (Fig. 7d), thereby encouraging the development of clay bridges. Elsewhere, the fibrous calcite forms meshworks on top of earlier clay bridges. In either case, it serves to reinforce the clay-bridge fabric. The very fine crystal size and the lack of interaction with roots and organic matter indicate that this acicular calcite was not formed within fungal mycelium (MA-type needle-fibre calcite), and it is coarser than bacterially-precipitated calcite microrods (M-type needle-fibre calcite) (cf. Verrecchia and Verrecchia 1994). However, tiny (<1 µm) rhombs of dolomite (its presence in the brickearth confirmed by XRD

analyses) occur in close association with this calcite, suggesting that this particular carbonate mineral assemblage and fabric was probably precipitated by evaporation of soil pore water fringes rather than having a biogenic origin.

Like the ‘non-calcareous’ brickearth, the calcareous brickearth also contains significant macroporosity in the form of abundant root hair channels. These are typically 0.2–1 mm diameter and form an intertwining network of channel-like cavities in the soil. In contrast to the ‘non-calcareous’ brickearth, these rootlet channels in the calcareous brickearth are not lined by needle-fibre calcite except in the top few centimetres of the unit. Instead, these open rootlet channels are surrounded by a halo of microcrystalline non-ferroan, non-manganous calcite cement that forms a tightly interlocking mosaic of xenomorphic (anhedral) crystals within the silt matrix (Fig. 7e). The silt particles are displaced and forced apart by the calcite producing an ‘expanded’ grain fabric (Fig. 7e). This calcite cement may penetrate into the silt for several millimetres from the root channel and patches of expanded-fabric calcite cement may develop into small calcrete nodules 1–4 mm in diameter. Some root channels may also be lined with finely laminated micritic calcite, which sometimes preserves the cellular fabric of the original root wall. Both vertical and horizontal calcified root channels display a similar expanded calcite cement fabric.

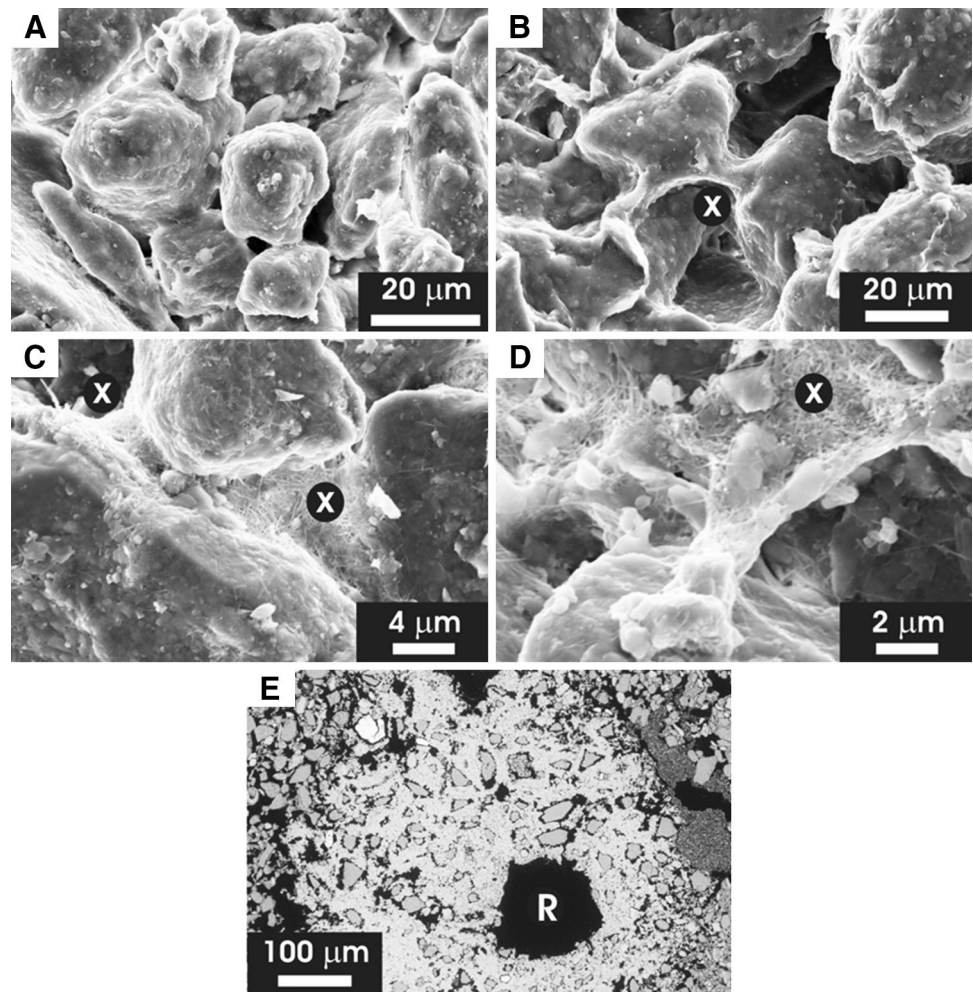
Limited observations of calcareous brickearth from the Star Lane and Cherry Orchard Lane sites in southeast Essex (see Fig. 1) appear to show similar grain fabrics to those seen in calcareous brickearth from Ospringe and Pegwell Bay.

## Geotechnical characteristics

### Geotechnical index properties

Geotechnical index data of disturbed samples taken within the upper and lower brickearths from the trial pit sections at Ospringe are presented in Table 4. All tests were undertaken in accordance with British Standard BS1377 (1990). These data confirm the more plastic (higher clay content) nature of the upper brickearth (liquid and plastic limits averaging 36 and 23 %, respectively), the lower brickearth being of low plasticity to non-plastic (liquid limits averaging 28 % and plastic limits ranging from 20 % to non-plastic). Water content profiles show values averaging 18–19 % for the upper brickearth and 12–13 % for the lower calcareous brickearth. The X-ray diffractometry carried out on the Ospringe brickearths indicates the clay mineral fraction is dominated by smectite throughout the sequence, with subordinate illite and kaolinite and minor quantities of chlorite. These clay minerals fall into the

**Fig. 7** Carbonate and clay fabric in the Calcareous Brickearth, Ospringle Pit 1. **a** SEM photomicrograph showing a loose packed framework of silt grains coated with a thick gelatinous film of clay. The clay forms meniscus 'bridges' between adjacent silt grains (2.26–2.35 m depth). **b** SEM photomicrograph showing well-developed meniscus clay 'bridge' bonding (x) between dispersed silt grains (2.39 m depth). **c** SEM photomicrograph showing fine needle calcite (x) forming a meniscus film bridging between adjacent silt grains (2.39 m depth). **d** SEM photomicrograph showing a meshwork of fine needle calcite forming a meniscus film (x) bridging between adjacent silt grains, and forming a 'scaffold' to support clay particles (2.39 m depth). **e** BSEM photomicrograph of calcite cement (rhizolithic calcrete) penetrating the silt adjacent to an open root hair channel (R). The calcite cement has forced apart the silt grains to produce an 'expanded' grain fabric (2.06 m depth)



grouping of 'active' or 'normal' clays (Skempton 1953). However, measured clay activities (Table 4) of 0.23–0.68, are similar throughout the upper and lower brickearth, are indicative of 'inactive' clays. This is consistent with a significant proportion of low-activity non-clay minerals being present in both brickearth horizons. As confirmed by the optical and SEM analyses, clay-grade quartz particles (with minor amounts of feldspars) make up a significant proportion of the brickearth clay fraction. In the calcareous brickearth, fine-grained secondary authigenic calcite also contributes to the 'inactive' clay size mineral fraction. Petrographic observations also show that iron oxide (or oxyhydroxide) and calcite act as cements, binding aggregations of clay-grade material into apparent coarser particles ('peds'), and inhibiting dispersion of fine silt and clay during particle size analysis.

#### Collapse potential

The collapse potential of the sampled brickearths was determined by undertaking single oedometer collapse tests on

undisturbed samples following the modified method described by Jennings and Knight (1975). Test specimens corresponding to a given depth were loaded at natural water contents up to pressures of 100, 200 and 400 kPa and then flooded. Following this, the specimens were incrementally loaded up to a pressure of 800 kPa. One test specimen from the lower calcareous brickearth at Ospringle Pit 2 was incrementally loaded at natural water content to 800 kPa before flooding. Metastable soils may be regarded as those that show a coefficient of collapse,  $C_{col}$  (defined as the change in volume or height of a specimen after flooding as a percentage of initial pre-collapse volume/height), of more than 1 % when flooded under imposed loading (Northmore et al. 1996).

The oedometer tests showed a clear distinction between the collapse potential of the upper and lower brickearths. The upper 'non-calcareous' brickearth showed no evidence of collapse under oedometer loadings, as indicated by  $C_{col}$  values ranging from 0 to 0.01 % for specimens flooded at 100 kPa and 0–0.02 % for specimens flooded at 200 and 400 kPa. However, similar collapse oedometer tests on the



**Table 4** Geotechnical index data for Ospringe Pit 1 and Pit 2 (data from Northmore et al. 2008)

| Trial pit no. | Depth (m) | Particle size (%) |      |      |      | Particle density (Mg/m <sup>3</sup> ) | Water content (%) | Liquid limit (%) | Plastic limit (%) | Plasticity index (%) | Activity | <425 $\mu$ m (%) | Lithology                 |
|---------------|-----------|-------------------|------|------|------|---------------------------------------|-------------------|------------------|-------------------|----------------------|----------|------------------|---------------------------|
|               |           | Gravel            | Sand | Silt | Clay |                                       |                   |                  |                   |                      |          |                  |                           |
| Pit 1         | 0.60      | 0.0               | 5.5  | 69.9 | 24.6 | 2.74                                  | 20.5              | 39               | 23                | 16                   | 0.65     | 98.7             | Non-calcareous brickearth |
|               | 0.80      | 0.1               | 11.4 | 58.7 | 29.8 | 2.61                                  | 18.2              | 37               | 23                | 14                   | 0.47     | 99.7             | Non-calcareous brickearth |
|               | 1.10      | 0.0               | 11.2 | 61.5 | 27.3 |                                       | 18.7              | 34               | 23                | 11                   | 0.40     | 99.8             | Non-calcareous brickearth |
|               | 1.30      | 0.0               | 20.2 | 60.6 | 19.2 | 2.71                                  | 17.9              | 37               | 24                | 13                   | 0.68     | 99.4             | Non-calcareous brickearth |
|               | 1.50      | 0.1               | 16.5 | 48.9 | 34.5 | 2.60                                  | 20.1              | 37               | 20                | 17                   | 0.49     | 99.8             | Non-calcareous brickearth |
|               | 1.85      | 0.0               | 15.8 | 54.0 | 30.2 | 2.70                                  | 19.1              | 36               | 23                | 13                   | 0.43     | 99.9             | Non-calcareous brickearth |
|               | 2.00      | 0.0               | 18.1 | 43.0 | 38.9 | 2.71                                  | 14.9              | 33               | 24                | 9                    | 0.23     | 99.9             | Non-calcareous brickearth |
|               | 2.20      | 0.0               | 16.5 | 68.6 | 14.9 | 2.71                                  | 14.4              | 27               | 21                | 6                    | 0.40     | 99.3             | Calcareous brickearth     |
|               | 2.40      | 0.1               | 26.9 | 55.5 | 17.5 | 2.71                                  | 10.9              | 29               | NP                | –                    | –        | 99.5             | Calcareous brickearth     |
|               | 2.90      | 11.3              | 34.9 | 35.4 | 18.4 | 2.65                                  | 11.9              | 27               | NP                | –                    | –        | 87.0             | Gravelly sandy brickearth |
|               | 3.40      | 0.0               | 21.6 | 56.8 | 21.6 | 2.69                                  | 17.5              | 31               | 19                | 12                   | 0.56     | 99.5             | Thanet Formation          |
| 3.70          | 0.7       | 12.0              | 68.9 | 18.4 | 2.68 | 19.9                                  | 34                | 23               | 11                | 0.60                 | 98.4     | Thanet Formation |                           |
| Pit 2         | 0.65      | 1.0               | 6.0  | 69.1 | 23.9 | 2.63                                  | 17.8              | 36               | 24                | 12                   | 0.50     | 98.2             | Non-calcareous brickearth |
|               | 1.60      | 0.0               | 12.7 | 56.9 | 30.4 | 2.65                                  | 19.1              | 38               | 23                | 15                   | 0.49     | 100.0            | Non-calcareous brickearth |
|               | 2.40      | 1.4               | 9.7  | 76.1 | 12.8 | 2.71                                  | 16.1              | 29               | 22                | 7                    | 0.55     | 97.7             | Calcareous brickearth     |
|               | 3.10      | 10.8              | 45.5 | 28.7 | 15   | 2.64                                  | 10.5              | 28               | 20                | 8                    | 0.53     | 87.8             | Gravelly brickearth       |
|               | 3.40      | 0.6               | 57.5 | 17.2 | 24.7 | 2.69                                  | 11.3              | 28               | 21                | 7                    | 0.28     | 99.2             | Thanet formation          |

lower calcareous brickearth at 2.5 m depth from Ospringe Pit 1 showed clear evidence of metastability. For these samples, coefficient of collapse values of 0.5, 4.2 and 5.3 % were obtained when flooded under pressures of 100 and 200 and 400 kPa, respectively.

It should be noted that the collapse potential of the lower calcareous brickearth showed some degree of variability across the Ospringe site. For example, oedometer collapse tests on a sample from 2.5 m depth at Ospringe Pit 2 (located c. 100 m north of Pit 1) recorded  $C_{col}$  values of 3 % when flooded at 100 and 200 kPa and only 0.8 % when flooded at 400 kPa. No collapse was recorded for the specimen from this location flooded at 800 kPa. This decrease in collapse strain at 400 kPa, reducing to zero at 800 kPa, would appear to reflect the ‘yielding’ or compression of the interparticle bonds (specifically the bridging clay bonds between quartz silt particles) during these higher loadings prior to flooding, thus decreasing voids ratios and the potential for rapid collapse.

Very similar results were obtained from oedometer collapse tests on upper and lower brickearth samples from Ospringe and from the Pegwell Bay cliff section (Fookes and Best 1969). Similar collapse behaviour was also recorded by Northmore et al. (1996) for brickearths in south Essex.

The collapse behaviour of these brickearths and the controlling influence of their mineralogy and soil fabrics on the collapse process is considered in more detail below.

#### In situ cone penetrometer and geophysical profiling

As part of the site assessment of the brickearth at the Ospringe site, in situ penetrometer profiling using a light-weight dynamic cone penetrometer to determine the dynamic cone resistance,  $q_d$  (see Langton 1999), and geophysical resistivity and shear wave profiling were carried out in order to ascertain property variations areally and with depth across the site. Particular emphasis was placed on tracing the depth and extent of the metastable lower brickearth horizon. The test methodologies and detailed results of these surveys across the Ospringe site are described by Northmore et al. (2008).

Typical penetrometer profile results obtained adjacent to Ospringe Pit 1 are shown in Fig. 8a. The profile shows a general decrease in  $q_d$  from about 5–2.5 MPa through the topsoil and upper brickearth to 0.5 m depth (possibly indicating a slightly desiccated surface layer). Below 0.5 m the  $q_d$  profile through the upper brickearth remains more or less constant around 2.5 MPa, only showing a slight decreasing trend with depth to 1.5 MPa. At the boundary with the underlying calcareous brickearth at c. 2.1 m,  $q_d$  values increase to c.3–3.5 MPa and continue to show a slightly increasing trend with depth to c. 4 MPa through the lower brickearth. The clear and continued increase in  $q_d$  values at the ‘non-calcareous’/calcareous brickearth boundary is mirrored by a corresponding decrease in natural water content and degree of saturation values (see Fig. 8c) at the

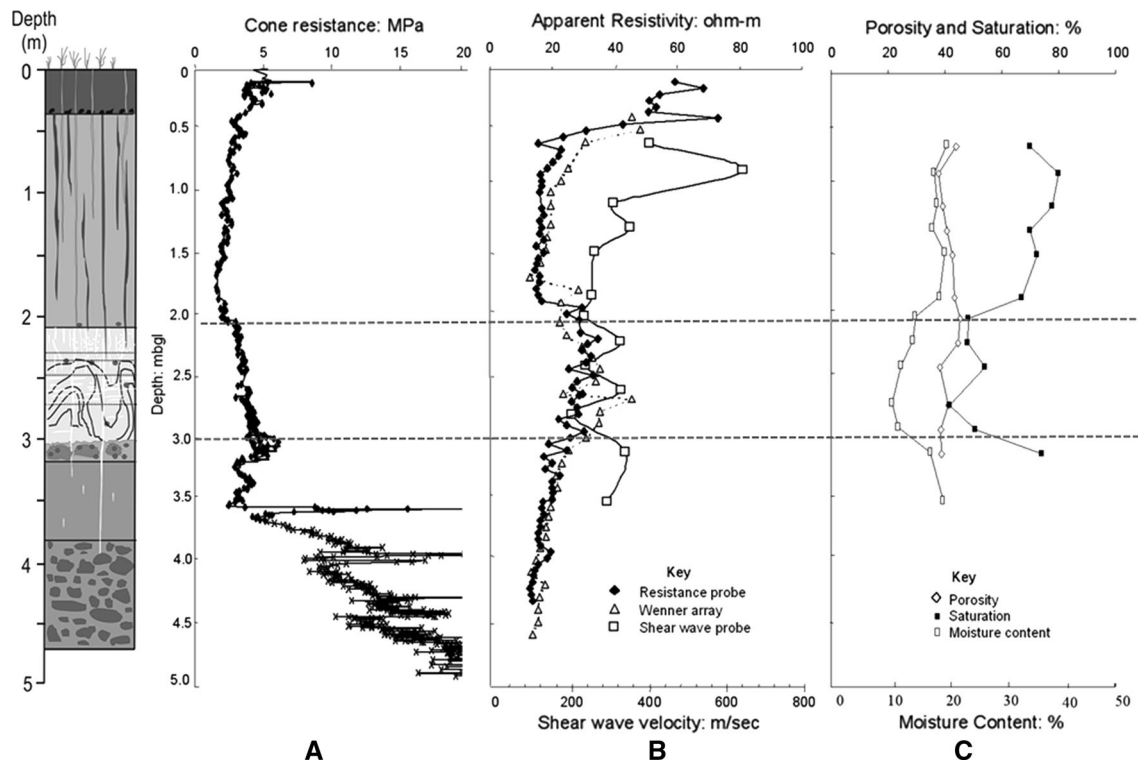


**Fig. 8** Ospringe Pit 1: lithological log in relation to (a) cone penetrometer, (b) resistivity and shear wave velocity, and (c) porosity, saturation, moisture content profiles (Northmore et al. 2008)

same boundary and through the full depth of the lower calcareous brickearth. The mottled sandy gravel layer marking the base of the brickearth sequence results in a further sharp and erratic increase in cone resistance ( $>5$  MPa) before assuming a constant, if slightly erratic, trend through the upper layers of the underlying sand facies of the Thanet Formation. Erratic rapid and large increases in  $q_d$  values in the mid-lower part of this sandy sequence result from the cone striking scattered flint clasts, a trend that becomes more marked in the basal section of the profile in the gravelly sands of the Bullhead Beds.

In situ resistivity profiling was carried out using a small hand-held Wenner array (configured with an electrode spacing of 10 cm) and a resistivity probe with measurements taken at 50 mm intervals down the trial pit faces. The probe was designed to be inserted down existing holes made by the cone penetrometer and enabled resistance point data to be recorded at 0.05 m intervals below ground surface (bgs) to depths of up to 3 m (Jackson et al. 2006). Benching of the trial pit excavations with guide holes made by the cone penetrometer from the benched surfaces enabled acquisition of a resistivity probe profile through the full depth of the trial pit. Close similarity between the apparent resistivity profiles determined by the probe and hand-held Wenner array is shown in Fig. 8b, where the

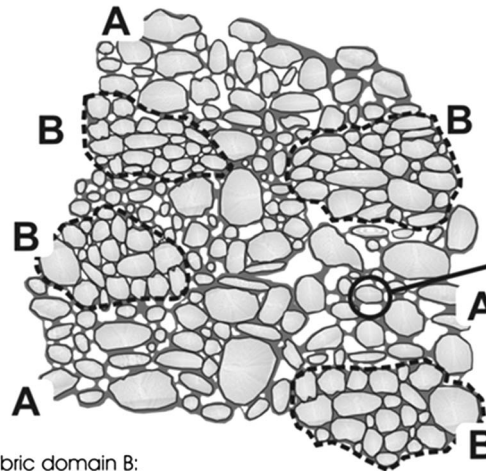
data can be related to the lithological, penetrometer and water content profiles. The resistivity profiles showed an overall distinction between the upper and lower loessic brickearths, the former consistently recording values of  $<20 \Omega\text{-m}$  compared to  $\sim 22\text{--}30 \Omega\text{-m}$  in the lower calcareous brickearth. Calcite was observed to occur in a number of forms in the calcareous brickearth, for example, as calcified rootlet channels and nodular calcite concretions. Therefore, taken together with the reduction in water content seen in Fig. 8c, this horizon must contain proportionately less conductive material than the upper brickearth, and an increase in resistivity is to be expected here. Calcrite nodules ranging up to 20–30 mm are a likely explanation for sudden ‘peak’ increases recorded in resistivity profiles within the calcareous brickearth.

Shear wave velocity data were acquired down a vertical face of Ospringe Pit 1 by a probe consisting of two small piezoelectric bender elements each attached to the end of 0.5 m long PVC tubes, one acting as a receiver and one as a transmitter. The transmitter–receiver pair was installed into pre-formed holes such that their flat faces shared the same plane, with a spacing of nominally 200 mm (Gunn et al. 2006). The data acquired indicate little variation in the lower 600 mm of the upper, ‘non-calcareous’ brickearth layer with greater variation above this interval (Fig. 8b).

**Fig. 9** Schematic summarising the essential elements of the collapsible brickearth microfabric. **a** Domains of open-packed silt/fine sand with widely separated grains held in place by a skeletal framework of meniscus clay bridges; **b** domains consisting of pelletised compacted clay/silt loosely stacked together

**Fabric domain A:**

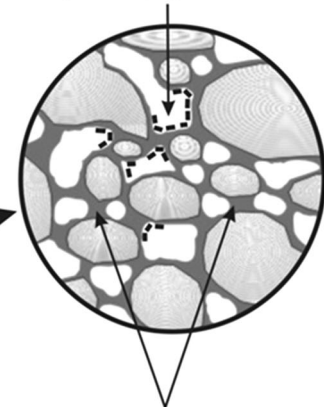
Open grain fabric of loosely-packed grains, supported by meniscus clay bridges forms a 'matrix' between Fabric B domains



**Fabric domain B:**

Discrete domains of close-packed grain fabric, with pore-filling and tangential grain coating clay, resemble ped-like features

Authigenic calcite and/or dolomite precipitated on the the surface of the clay meniscus strengthens the 'grain-bridging' clay



Grain-coating clay meniscus around grains forms 'bridges' across pore throats and supports an open, loosely-packed grain framework in fabric domain type A

The velocity variation in the interval from 0.7 to 1.2 m in the upper 'non-calcareous' brickearth is likely to be caused by changes in the material stiffness. Higher velocities are associated with material of increased stiffness possibly due to greater compaction or stronger cementation (possibly related to desiccation) of the upper brickearth fabric. For example, an examined thin section of material from 0.7 m depth showed a cemented fabric. Whereas, a thin section from 1.79 m bgs showed a very porous fabric, with abundant macroporosity present in the form of old rootlet channels, with larger root channels containing relict fibrous organic remains, possibly of decayed root material.

The profile data also indicate marked variation within the whole of the lower calcareous brickearth layer below c. 2.0 m, again due to changes in material stiffness. This may be explained by the shear wave velocity responding to the effect of nodular calcite, calcified rootlet development and irregular calcitic 'cementation' between silt-sized quartz particles forming the brickearth fabric. For example, a thin section from c. 2.1 m depth shows micronodular calcite cement in a quartz silt dominant matrix, displaying an 'expanded' silt grain fabric caused by displacement of silt grains during calcite nodule growth (Fig. 7e). A sample from 2.35 m had a fine-grained, very open and diffuse calcite cement within fine silt, which preserves a fabric with open root channels. Thus, the highly variable shear wave velocity data appear to be consistent with the calcareous brickearth fabric being relatively heterogeneous in comparison with that of the upper 'non-calcareous' brickearth.

### Mineralogical and fabric influences on engineering behaviour

The basic soil properties of particle size, mineralogy, fabric, interparticle bonding, density and water content determine the geotechnical and geophysical responses of soil. This is reflected in the geotechnical, penetrometer and geophysical data acquired through the upper and lower brickearth sequences at Ospringe. Of particular interest are the effects of mineralogical and soil fabric on rapid collapse settlement and the marked differences in the collapse behaviour between the lower and upper brickearths (Northmore et al. 2008; Gunn et al. 2006; Jackson et al. 2006; Zourmpakis et al. 2006).

The difference in collapse behaviour between the upper 'non-calcareous' and lower calcareous brickearths at Ospringe can be explained by significant differences in their mineral microfabrics. As described above, the non-collapsing upper brickearth is characterised by a close-packed grain fabric of tightly interlocked silt/sand grains, in which a high proportion of the grains are in direct grain-to-grain contact (Figs. 5c, e, f, 6a). Any load applied to the soil would be taken up primarily via grain-to-grain contact between competent and rigid (dominantly quartz) silt grains. Collapse of macroporous root channels may occur but these are volumetrically small and would give rise to only minor collapse. Extensive meniscus clay films are present but largely as drapes around silt grains that are already in close point contact, and play no role in supporting the applied load. Therefore, if the clay were

dispersed on saturation this would have very little impact on the collapse behaviour of the sediment. Because the silt/sand grains are already close-packed and interlocked (Fig. 5f), there is also limited space for any physical rearrangement of grains to accommodate tighter packing. Consequently, this type of brickearth fabric exhibits little or no collapse under saturated loading conditions. Wetting might even result in a slight increase in volume if sufficient smectitic (swelling) clay was present (Table 3). This phenomenon might account for the slight swelling observed in collapse tests on addition of water for some brickearths from Essex (Northmore et al. 1996) and from Kent (Derbyshire and Mellors 1988).

The collapsible lower calcareous brickearth has a more complex structure, comprising two discrete microfabric elements, as demonstrated by fabric observations discussed above in Sect. 5, which will differ in their mechanical properties. Figure 9 provides a useful conceptualisation of these essential elements that make up the brickearth microfabric. Within the domains of pelletised silt/clay, comprised of tightly packed clay-coated silt grains (fabric domain B, Fig. 9), loading will largely be borne by grain-to-grain contacts. In contrast, the open-packed silt/sand filling the inter-pelletal domains (fabric domain A, Fig. 9) have a very high voids ratio, and the silt grains are widely-separated by clay bridges with little direct grain-to-grain contact. In these domains, the applied load is primarily supported by the delicate clay bridges or buttresses that hold the silt particles and adjacent peds in position. Wetting and saturation will cause the clay forming the bridges to soften, disperse and disrupt. Similar behaviour was also observed in loess soils by Klukanova and Sajgalik (1994). The silt grains will then be unsupported and collapse will ensue. Disruption of the clay bridges will be greatly enhanced when smectite is a significant component of the clay (as in the north Kent brickearths) because this will adsorb significant interlayer water and cause the clay fabric to swell and weaken.

Petrographical evidence indicates that collapse on saturation could occur in up to three stages:

- Stage 1. Dispersion and disruption of clay bridges or buttresses between loosely-packed silt grains, leading to initial rapid collapse of the inter-ped matrix silt (fabric domain A, Fig. 9);
- Stage 2. After Stage 1, any load will be taken up via the contacts between adjacent compacted silt peds (fabric domain B, Fig. 9) and the peds will re-organise into a closer packing;
- Stage 3. With increasing load, progressive deformation and shearing of the peds will occur, with further collapse as the peds disaggregate and the component silt particles collapse into the now-unsupported inter-ped regions.

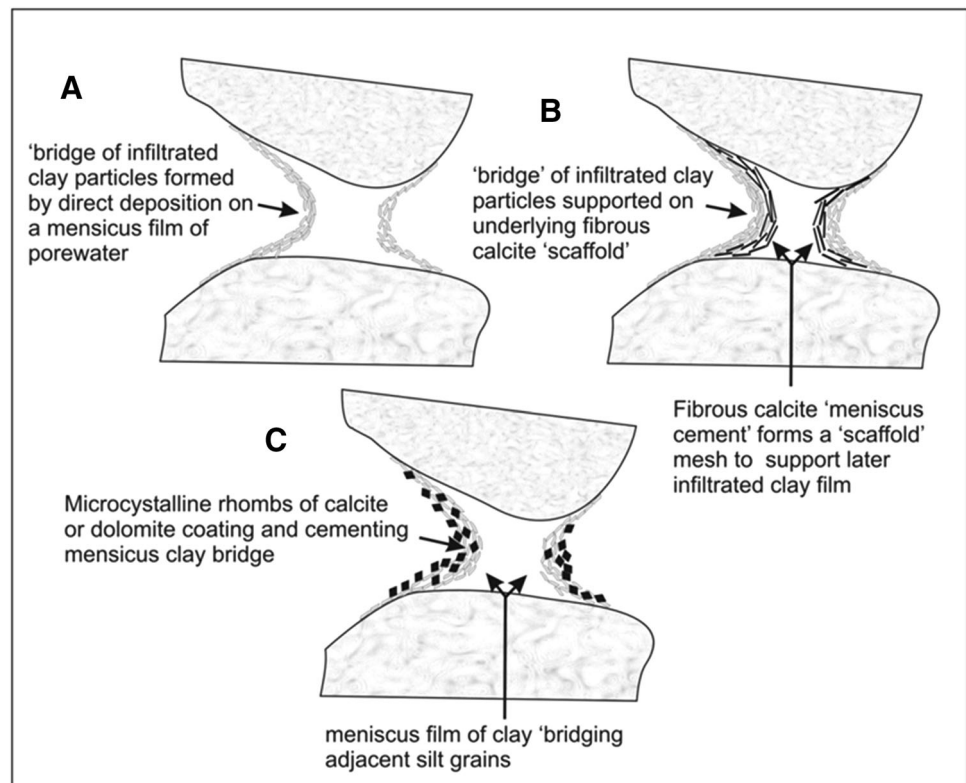
Wetting and saturation will potentially enhance ped disaggregation in Stage 3 by causing dispersion of the clay binding the component silt particles within the peds. SEM examination of samples of brickearth after flooding collapse in oedometer tests, and collected following the Ospringe field collapse trial, reveals the brickearth has been modified to a largely close-packed grain framework similar to that seen in the 'non-calcareous' brickearth. However, traces of the original ped fabrics can still be discerned, and this indicates that Stage 3 did not achieve the maximum possible state of consolidation settlement under the loads applied in either the field and laboratory tests.

Results from oedometer collapse tests showed that the potential for the calcareous brickearth fabric to collapse can be reduced or destroyed if pre-flooding loads result in yielding or compression of the bridging clay bonds between the quartz silt particles. This will result in a decrease in voids ratio, an increase in grain to grain contacts and thus a reduced potential for rapid collapse. Although only minimal or no collapse was consistently recorded for the Ospringe brickearths under pre-flooding loads of 800 kPa, loadings of 400 k Pa on the samples tested showed both reduced and increased values of collapse. This is perhaps indicative of variations in the soil fabric and calcite cementation across the site.

Carbonate diagenesis could have some influence on the collapse behaviour of the brickearth. Calcite and dolomite cements may strengthen the meniscus clay bridges between silt grains and help to bind the grains together. Three variants of clay bridge fabric can be defined in the metastable brickearth based on fabric studies discussed in Sect. 5 (Fig. 10): (a) simple clay bridges with no carbonate mineralisation; (b) clay bridges that are formed by deposition of a meniscus of clay supported on a scaffold meshwork of needle-fibre calcite deposited as an earlier meniscus film between grains (as shown in Fig. 7d); and (c) clay bridges that have been encrusted and impregnated by later micritic calcite and dolomite. The carbonate mineralisation in type (b) and type (c) will reinforce the clay bridges and potentially reduce dispersion of the clay upon wetting. However, both of these fabrics are relatively minor features and most of the clay bridges present in the collapsing brickearth are of type (a). This is important because it shows that the carbonate mineral fabrics are not an essential feature of the collapsing brickearth.

Micritic and microsparry calcite cementation associated with the replacement (calcification) of ancient roots and the development of patchy nodular calccrete cements may strengthen the soil fabric locally and reduce compaction. This is evident from SEM observations of the post-collapse brickearth fabric in field and laboratory tests, which show the relatively large voids in calcareous root channels are still preserved in the post-collapse soil. These have been

**Fig. 10** Schematic illustrating three types of clay bridge fabric discriminated in collapsing brickearth: **a** simple clay meniscus films; **b** clay films developed on a scaffold of an earlier meniscus precipitate of fibrous calcite; **c** clay films permeated or encrusted by microcrystalline (micritic) calcite and/or dolomite



kept open by the presence of the rhizolithic calcrete cement that binds the peds and silt particles in the walls of these features.

#### Relationship between calcareous and 'non-calcareous' brickearth and the development of the metastable brickearth fabric

It is important to consider how the metastable brickearth fabric developed in order to understand the distribution of collapsible loessic deposits. The role of grain bridging clay and clay buttress structures in binding the metastable silt grain fabric has been identified in previous studies of brickearth and other loessic deposits (Derbyshire et al. 1994; Derbyshire and Mellors 1988; Northmore et al. 1996; Bell et al. 2003). Derbyshire and Mellors (1988) commented that clay buttresses, formed between widely separated grains, might be indicative of in situ aeolian deposits, since such features would be destroyed by reworking in running water, slurry flow or solifluction. Gao (1988) also recognised the importance of a loose-packed aggregate grain framework in collapsible loess from China. He attributed aggregate grain formation to a 'loessisation' process involving flocculation of clay/silt particles during wetting under humid conditions, followed by stabilization of the aggregates by weak carbonate cements precipitated

during arid periods. Both of these fabric elements are important in the metastable brickearth from north Kent (and in the more limited samples examined from south Essex).

Gao (1988) suggested that loess might lose its metastability through softening and destruction of the pelloidal fabric during weathering and by leaching of the carbonate cements under wetter climatic conditions. Previous studies have also suggested that the upper, darker, 'non-calcareous' brickearth in Kent represents the decalcified or leached top of the calcareous brickearth, and that these two types of brickearth are contemporaneous (Kerney 1965; Weir et al. 1971; Catt 1988; Derbyshire and Mellors 1988; Antoine et al. 2003). However, this does not account for the differences in properties between the upper (non-collapsible) 'non-calcareous' brickearth and lower (collapsible) calcareous brickearth from the two areas of north Kent examined in the present study.

The present study has found no evidence for decalcification in the upper unit. Despite being described as 'non-calcareous,' our petrographical analyses show that primary detrital carbonate grains (including reworked detrital clasts of chalk and foraminifera fragments in a micritic calcite matrix) are present as accessory components and that they display no evidence of corrosion or dissolution. This study has found evidence to indicate that 'non-calcareous' brickearth and calcareous brickearth are discretely different sedimentary units. An erosion surface at the junction

between the two units can clearly be seen in the sedimentary profiles at both study sites. This is defined by a sharp colour change and truncation of calcified root structures and associated rhizolithic calcrete at the top of the calcareous brickearth. Further detailed SEM observations of silt/fine sand quartz surfaces (following removal of clay cutans by ultrasonic cleaning) show that the morphological characteristics of the quartz grains (the major component of the sediment) are different between the two brickearth horizons (Fig. 11). There is a decrease in the proportion of corroded quartz grains from the Thanet Formation through the calcareous brickearth to the 'non-calcareous' brickearth. However, the most striking difference is in the relative proportions of angular grains with sharp edges and abraded or rounded grains. About 50 % of the silt/fine sand in the upper 'non-calcareous' brickearth are angular grains with sharp edges, whilst <20 % of the grains are abraded with rounded edges. This is in marked contrast with the lower calcareous brickearth, where approximately 50 % of the silt/fine sand are rounded and abraded, whereas <25 % of the grains are angular with sharp edges. Similar results were found for both the Ospringe and the Pegwell Bay sites. The silt/sand grain characteristics in the calcareous brickearth show more similarity to those found in the underlying Thanet Formation, suggesting that reworking of these local strata may have provided much of the quartz silt for the calcareous brickearth sediment. In contrast, the much higher proportion of angular silt/sand in the 'non-calcareous' brickearth would probably be more consistent with a dominant source of angular silt freshly derived from distal glacial material (cf. Krinsley and Doornkamp 1973) re-worked from outwash sandurs in the North Sea Basin area. Furthermore, OSL dating of samples from immediately above and immediately below the junction between the two types of brickearth also points to them being of significantly different age at both sites (Table 5).

The formation of a metastable fabric in the calcareous brickearth of north Kent may be related to periglacial freeze–thaw processes. Evidence of cryoturbation of clay laminae was observed in the calcareous brickearth from Ospringe (Fig. 2) and extensive frost-shattering can be seen in the underlying chalk and Thanet Formation at Pegwell Bay (Kerney 1965). Micromorphological fabrics, including silt/clay-capped coarse grains, pelletised ferri-argillans ('papules,' cf. Tarnocai and Smith 1989) and plasmic clay fragments found in the 'non-calcareous' brickearth are characteristic of cold climate/permafrost soils; they are formed by repeated freeze–thaw (Kemp 1985, 1987; Rose et al. 1985; Van Vliet-Lanoë 1985), and are consistent with cryoturbation observed at Ospringe. Freeze/thaw and cryodesiccation of clay-rich soils can also produce grain aggregation, and once produced these

aggregates can be difficult to disperse when the ice melts because they have been compacted by expanding ice crystals in the soil (Van Vliet-Lanoë 1985). The action of porewater solutes may also be very important in stabilising the aggregates. Freezing increases salt concentration in the porewater and encourages flocculation of clay minerals. Very stable aggregates can be produced by these processes and are frequently re-worked in fluvial or colluvial deposits, forming soft pellets (Van Vliet-Lanoë 1985). Cavities (vesicles) commonly form in soils subject to freezing and thawing caused either by air expulsion or crystal 'heave' during ice growth; significant inter-particle and inter-aggregate porosity can arise (Fitzpatrick 1956; Coutard and Mùcher 1985; Van Vliet-Lanoë 1985). On thawing, meltwater can percolate deep into the soil profile. The high dielectric properties of this water can cause dispersion of weakly stabilised aggregates and result in macro- and micro-erosion within the soil profile. In turn, this can allow illuvial transport and accumulation at depth of fine particles ranging from clays (if the pH is neutral) to silt and fine sand (Van Vliet-Lanoë 1985). These periglacial processes could potentially have produced the fabrics observed in the calcareous brickearth of north Kent, with the pelletisation and grain aggregation coupled with development of a loose-packed ped structure occurring during freezing, and translocation and illuvial transport and deposition of clay cutans, clay bridges and loose inter-ped-silt taking place during thawing cycles.

The upper 'non-calcareous' brickearth could represent a head or solifluction deposit that has moved or 'sludged' across the lower calcareous sequence from higher ground, although there may have been erosion and some period of time preceding its emplacement (Holmes 1981). The poor zeroing of the OSL data for this material (Clarke et al. 2007) might also support this suggestion. The low plasticity indices of the brickearth materials (Northmore et al. 1996, 2008) indicate that they are prone to lose strength and flow when water contents are high, particularly in a saturated surface layer overlying otherwise frozen ground. This process would have destroyed any cryogenic fabrics that may have originally been present and may be responsible for the lack of metastability. There is no petrographical evidence of any fabrics that might indicate alluvial reworking of loess in the upper 'non-calcareous' brickearth at the two study sites.

## Conclusions

Detailed mineralogical and petrographical analysis of two brickearth profiles from Ospringe and Pegwell Bay in north Kent (supplemented by limited observations from other brickearth deposits in southern England) have differentiated

**Fig. 11** Variation in the proportion of quartz silt grains with different morphological characteristics in the brickearth and Thanet Formation from Ospringe

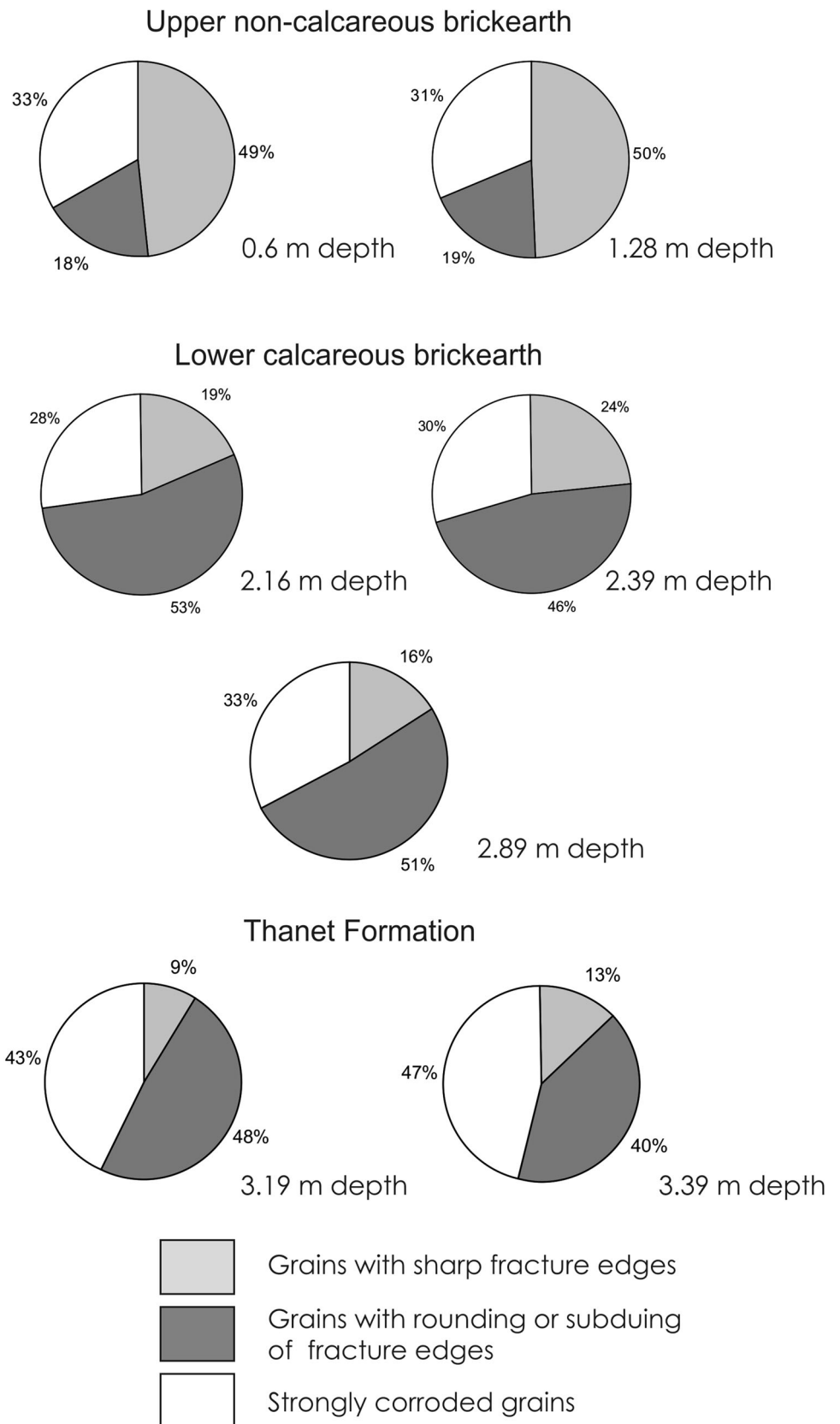


**Table 5** OSL ages determined for 38–53  $\mu\text{m}$  quartz grains from Ospringe and Pegwell Bay brickearth deposits (Clarke et al. 2007)

| Site           | Sample | Depth (m) | Horizon                   | OSL age (years)    |
|----------------|--------|-----------|---------------------------|--------------------|
| Ospringe Pit 2 | OSP18  | 2.0       | Non-calcareous brickearth | 18,700 $\pm$ 2,290 |
| Ospringe Pit 2 | OSP19  | 2.5       | Calcareous brickearth     | 23,760 $\pm$ 1,300 |
| Pegwell Bay    | PB14   | 0.99      | Non-calcareous brickearth | 14,990 $\pm$ 860   |
| Pegwell Bay    | PB15   | 1.44      | Calcareous brickearth     | 17,215 $\pm$ 1,305 |

two types of brickearth fabric that can be correlated with their different engineering behaviour. The brickearth sequence at both study sites comprises metastable (collapsing) calcareous brickearth overlain by non-collapsing 'non-calcareous' brickearth. Although previous studies have suggested that the upper horizon is the leached and decalcified equivalent of the underlying calcareous unit, this study has found no evidence for decalcification. Instead we demonstrate the two types of brickearth are discretely different units. There is clear evidence for an erosional contact between the two units, with the development of a palaeosol horizon at the top of the calcareous brickearth, associated with the formation of rhizolithic calcrete, indicative of soil formation under arid or semi-arid conditions. The lower calcareous brickearth also has mineralogical characteristics that indicate that a significant proportion of the sediment has been derived from the local Thanet Formation sand, whereas the upper 'non-calcareous' brickearth has characteristics that suggest a higher component of material derived from glacial detritus (probably sourced from the North Sea Basin). Significant differences in OSL dates obtained from above and below the junction between the two brickearths (Clarke et al. 2007) also lend support for the two types of brickearth being of different origin.

The lower calcareous brickearth is characterised by a fabric comprising an open-packed arrangement of pelleted aggregate grains or peds (consisting of compacted silt/clay). This is supported by an inter-ped matrix of loose-packed silt/fine sand grains held in place by an extensive and rigid skeletal framework of illuviated clay that form meniscus clay bridges and pillars between the component silt/sand grains. The silt/sand grains are entirely surrounded by thick clay cutans. There is little direct grain-to-grain contact and the brickearth has a very high void ratio. Any applied load is largely supported by these delicate meniscus clay bridge and pillar microfabrics. Collapse of this brickearth can be explained by a sequence of process involving: (1) dispersion and disruption of the grain-bridging clay upon saturation, leading to initial rapid collapse of the loose-packed inter-ped silt/sand; (2) rearrangement and closer stacking of the compact aggregate silt/clay peds; (3) with increasing stress, further consolidation may result from the deformation and break up of the peds as they collapse into the inter-ped regions. The presence of

significant smectite within the clay component will serve to aid dispersion and disruption of these clay fabrics as the smectite will swell on wetting. In contrast, the fabric of the 'non-calcareous' brickearth already possesses a close-packed and interlocking arrangement of silt/sand grains. Consequently, there is virtually no physical space for rapid collapse when saturated under applied loadings.

Minor calcite and dolomite mineralisation may also form meniscus cements between silt grains. These have either acted as scaffolds on which illuviated clay has subsequently been deposited or have encrusted earlier-formed grain-bridging clay. In either case the carbonates may help to reinforce the clay bridge fabrics. However, these carbonate features are a relatively minor feature and not an essential component of the collapsible brickearth fabric.

The origin and development of the metastable brickearth fabric is potentially important for understanding the distribution of collapsible brickearth. Evidence of cryoturbation and micromorphological features observed in thin sections suggests that the calcareous brickearth fabric has been influenced by periglacial freeze–thaw processes. Freezing, coupled with illuviation of clay during thawing, is probably responsible for forming the metastable pelleted and loose-packed clay-bridge grain fabrics now present. In contrast, the upper 'non-calcareous' brickearth may represent a head or solifluction deposit. Mass movement during solifluction will have destroyed any delicate grain-bridging clay microfabrics if they were originally present in this material.

The approach taken in this study to identify and explain the formation of collapsible and non-collapsible fabrics present in the loessic brickearth from north Kent is applicable to other loessic deposits. Such microfabric studies and the soil structures defined are fundamental for understanding and assessing the collapse potential and mechanisms involved when these deposits are saturated under engineering loads, and are of critical importance for designing and implementing appropriate remedial measures to mitigate the effects of such collapse.

**Acknowledgments** This project was undertaken as part of the BGS Core Programme Engineering Properties of UK Rocks and Soils Project, and the authors gratefully acknowledge the financial support from the Natural Environment Research Council (NERC grant reference GR3/12080). The authors also thank the Cremer Whiting



Company for permission to access and sample the Brickearth at the Ospringe Brickworks pit and for the provision of excavation plant equipment. Jon E. Bouch and John A. McKervey are thanked for their assistance with fieldwork and XRD analyses, respectively. This paper is published with the permission of the Executive Director of the British Geological Survey (NERC).

**Open Access** This article is distributed under the terms of the Creative Commons Attribution License which permits any use, distribution, and reproduction in any medium, provided the original author(s) and the source are credited.

## References

- Antoine P, Catt J, Lautridou J-P, Sommé J (2003) The loess and cover sands of northern France and southern England. *J Q Sci* 18:309–318
- Ballantyne CK, Harris C (1993) *The periglaciation of Great Britain*. Cambridge University Press, Cambridge
- Bates MR, Keen DH, Lautridou JP (2003) Pleistocene marine and periglacial deposits of the English Channel. *J Q Sci* 18:319–337
- Becze-Deák J, Langhort R, Verrechia EP (1997) Small scale secondary CaCO<sub>3</sub> accumulations in selected sections of the European loess belt. Morphological forms, and potential for palaeoenvironmental reconstruction. *Geoderma* 76:221–252
- Bell FG, Culshaw MG (2001) Problem soils: a review from a British perspective. In: Jefferson I, Murray EJ, Faragher E, Fleming PR (eds.) *Problematic soils*. Thomas Telford, London, pp 1–35
- Bell FG, Culshaw MG, Northmore KJ (2003) The metastability of some gull-fill materials from Allington, Kent, UK. *Q J Eng Geol Hydrogeol* 36:217–229
- British Standard BS1377-1 (1990) *Methods of tests for soils for civil engineering purposes. General requirements and sample preparation*. British Standards Institution, London
- Candy I (2002) Formation of a rhizogenic calcrete during glacial stage (Oxygen Isotope Stage 12): its palaeoenvironmental and stratigraphic significance. *Proc Geol Assoc* 113:259–270
- Carter DL, Heilman MD, Gonzalez FL (1965) Ethylene glycol monoethyl ether for determining surface area of silicate minerals. *Soil Sci* 100:356–360
- Catt JA (1977) Loess and coversands. In: Shotton F (ed) *British quaternary studies: recent advances*. Clarendon Press, Oxford, pp 221–229
- Catt JA (1988) Soils and Quaternary stratigraphy in the United Kingdom. In: Boardman JW (ed) *Quaternary geology for scientists and engineers*. Ellis Horwood, Chichester, pp 161–178
- Cattell AC (1997) The development of loess-bearing profiles on Permian Breccias in Torbay. *Proc Usher Soc* 9:168–172
- Clarke ML, Milodowski AE, Bouch JE, Leng MJ, Northmore KJ (2007) New OSL dating of UK loess: indications of two phases of Late Glacial dust accretion in SE England and climate implications. *J Q Sci* 22:361–371
- Coutard JP, Mûcher HJ (1985) Deformation of laminated silt loam due to repeated freezing and thawing cycles. *Earth Surf Proc Land* 10:309–319
- Derbyshire E, Mellors TW (1988) Geological and geotechnical characteristics of some loess and loessic soils from China and Britain: a comparison. *Eng Geol* 25:135–175
- Derbyshire E, Dijkstra TA, Smalley IJ, Li Y (1994) Failure mechanisms in loess and the effects of moisture content changes on remoulded strength. *Quatern Int* 24:5–15
- Dines HG, Holmes SCA, Robbie JA (1954) *Geology of the Country around Chatham*. Memoir Geol Surv, United Kingdom, HMSO, London
- Fitzpatrick EA (1956) An indurated soil horizon formed by permafrost. *J Soil Sci* 7:248–254
- Fookes PG, Best R (1969) Consolidation characteristics of some late Pleistocene periglacial metastable soils of east Kent. *Q J Eng Geol* 2:103–128
- Gao G (1988) Formation and development of the structure of collapsing loess in China. *Eng Geol* 25:235–245
- Gunn DA, Nelder LM, Jackson PD, Northmore KJ, Entwisle DC, Milodowski AE, Raines MR, Boardman DI, Zourmpakis A, Rogers CDF, Dixon N, Jefferson I, Smalley IJ, Karri RS, Rouaiguia A (2006) Shear wave velocity monitoring of collapsible Brickearth soil. *Q J Eng Geol Hydrogeol* 39:173–188
- Holmes, SCA (1981) *Geology of the country around Faversham*. Memoir of the British Geological Survey, Sheet 273, pp 117
- Jackson PD, Northmore KJ, Entwisle DC, Gunn DA, Nelder LM, Milodowski AE, Raines MR (2006) Electrical resistivity monitoring of a collapsing meta-stable soil. *Q J Eng Geol Hydrogeol* 39:151–172
- Jefferson I, Tye C, Northmore KJ (2001) Behaviour of silt: the engineering characteristics of loess in the UK. In: Jefferson, I, Murray EJ, Faragher E, Fleming PR (eds.) *Problematic Soils*. Thomas Telford, London, pp 37–52
- Jefferson I, Smalley IJ, Northmore KJ (2003) Consequences of a modest loess fall over southern and midland England. *Mercian Geol* 15:199–208
- Jennings JE, Knight K (1975) A guide to construction on or with materials exhibiting additional settlement due to collapse of grain structure. In: *Proceedings of the 6th African Conference on Soil Mechanics and Foundation Engineering*, Durban, pp 99–105
- Kabanov PB (2005) Traces of terrestrial biota in the Upper Moscovian paleosols of central and northern European Russia. *Paleontol J* 39:372–385
- Kemp RA (1985) The Valley Farm Soil in southern East Anglia. In: Boardman J (ed) *Soils and Quaternary Landscape Evolution*. Wiley, Chichester, pp 179–196
- Kemp RA (1987) Interpretation and environmental significance of a buried Middle Pleistocene soil near Ipswich Airport, Suffolk, England. *Philos Trans R Soc Lond B* 317:365–391
- Kerney MP (1965) Weischelian deposits in the Isle of Thanet, east Kent. *Proc Geol Assoc* 76:269–274
- Klukanova A, Sajgalik J (1994) Changes in loess fabric caused by collapse: an experimental study. *Quatern Int* 24:35–39
- Knox, RWO'B (1979) Igneous grains associated with zeolites in the Thanet Beds of Pegwell Bay, northeast Kent. *Proc Geol Assoc* 90:55–60
- Krinsley DH, Doornkamp JC (1973) *Atlas of Quartz Sand Surface Textures*. Cambridge University Press, London 91 pp
- Langton DD (1999) The Panda lightweight penetrometer for soil investigation and monitoring material compaction. *Ground Eng*, 31(9), pp 33–37
- Large DJ, Fortey NJ, Milodowski AE, Christy AG, Dodd J (2001) Petrographic observations of iron, copper, and zinc sulfides in freshwater canal sediment. *J Sediment Res* 71:61–69
- Moore DM, Reynolds RC (1997) *X-ray diffraction and the Identification and analysis of clay minerals*, 2nd edn. Oxford University Press, New York
- Northmore KJ, Bell FG, Culshaw MG (1996) The engineering properties and behaviour of the brickearth of South Essex. *Q J Eng Geol Hydrogeol* 29:147–161
- Northmore KJ, Jefferson I, Entwisle DC, Gunn DA, Jackson PD, Raines MG, Milodowski AE, Boardman D, Dixon N, Rogers CDF, Smalley IJ, Zourmpakis A (2008) On-site characterisation of loessic deposits at Ospringe, Kent. *Geotechnical Engineering* 161, February 2008, Issue GE1, 3–17
- Parks DA, Rendell HM (1988) TL dating of brickearth from SE England. *Quatern Sci Rev* 7:305–308

- Parks DA, Rendell HM (1992) Thermoluminescence dating and geochemistry of loessic deposits in southeast England. *J Quat Sci* 7:99–107
- Phillips SE, Self PG (1987) Morphology, crystallography and origin of needle-fibre calcite in Quaternary pedogenic calcretes of South Australia. *Aust J Soil Res* 25:429–444
- Pitcher WS, Shearman DJ, Pugh DC (1954) The loess of Pegwell Bay and its associated frost soils. *Geol Mag* 91:308–314
- Reynolds RC, Reynolds RC (1996) Description of Newmod-for-Windows™. The calculation of one-dimensional X-ray diffraction patterns of mixed layered clay minerals. R C Reynolds, 8 Brook Road, Hanover, NH 03755, USA
- Rogers CDF, Dijkstra TA, Smalley IJ (1994) Hydroconsolidation and subsidence of loess: studies from China, Russia, North America and Europe. *Eng Geol* 37:83–113
- Rose J, Allen P, Kemp RA, Whiteman CA, Owen N (1985) The Early Anglian Barnham Soil of Eastern England. In: Boardman J (ed) *Soils and Quaternary Landscape Evolution*. Wiley, Chichester, pp 197–229
- Skempton, AW (1953) The colloidal 'activity' of clays. In: *Proceedings of the 3rd International Conference on Soil Mechanics and Foundation Engineering*, Zurich, pp 57–61
- Strong GE, Giles JE, Wright VP (1992) A Holocene calcrete from North Yorkshire, England: implications for interpreting palaeoclimates using calcretes. *Sedimentology* 39:333–347
- Tarnocai C, Smith CAS (1989) Micromorphology and development of central Yukon palaeosols, Canada. *Geoderma* 45:145–162
- Van Vliet-Lanoë B (1985) Frost effects in soils. In: Boardman J (ed) *Soils and quaternary landscape Evolution*. Wiley, Chichester, pp 117–158
- Verrecchia EP, Verrecchia KE (1994) Needle-fibre calcite: a critical review and a proposed classification. *J Sediment Res* A64:650–664
- Weir AH, Catt JA, Madgett PA (1971) Postglacial soil formation in the loess of Pegwell Bay, Kent (England). *Geoderma* 5:131–149
- Wright VP (1984) The significance of needle-fibre calcite in a lower carboniferous palaeosol. *Geol J* 19:23–32
- Wright VP (1986) The role of fungal biomineralization in the formation of early carboniferous soil fabrics. *Sedimentology* 33:831–838
- Zourmpakis A, Boardman DI, Rogers CDF, Jackson PD, Gunn DA, Northmore KJ, Entwisle DC, Dixon N, Milodowski AE, Raines MR, Nelder LM, Jefferson I, Smalley IJ, Rouaiguia A, Karri RS, Derbyshire E (2006) A case study of loess collapse in a UK field trial. *Q J Eng Geol Hydrol* 39:131–150